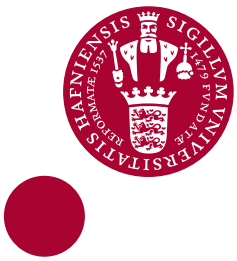

# A new set-up for simultaneous high-precision measurements of CO2,13 C-CO2 and 18O-CO2 on small ice core samples

Jenk, Theo Manuel; Rubino, Mauro; Etheridge, David; Ciobanu, Viorela Gabriela; Blunier, Thomas

*Published in:*
Atmospheric Measurement Techniques

*DOI:*
10.5194/amt-9-3687-2016

*Publication date:*
2016

*Document version*
Publisher's PDF, also known as Version of record

Atmos. Meas. Tech., 9, 3687–3706, 2016
www.atmos-meas-tech.net/9/3687/2016/
doi:10.5194/amt-9-3687-2016


Atmospheric Measurement Techniques
Open Access
EGU

# A new set-up for simultaneous high-precision measurements of $CO_2$, $\delta^{13}$C-$CO_2$ and $\delta^{18}$O-$CO_2$ on small ice core samples

**Theo Manuel Jenk**[1,a], **Mauro Rubino**[2,b], **David Etheridge**[2], **Viorela Gabriela Ciobanu**[1], **and Thomas Blunier**[1]

[1]Centre for Ice and Climate, Niels Bohr Institute, University of Copenhagen, Copenhagen, Denmark
[2]CSIRO Oceans and Atmosphere, Aspendale, Victoria, Australia
[a]now at: Paul Scherrer Institute, Laboratory of Environmental Chemistry, Villigen PSI, Switzerland
[b]now at: Seconda Università degli Studi di Napoli, Caserta, Italy

*Correspondence to:* Theo Manuel Jenk (theo.jenk@psi.ch)

Received: 13 November 2015 – Published in Atmos. Meas. Tech. Discuss.: 1 February 2016
Revised: 16 May 2016 – Accepted: 21 June 2016 – Published: 10 August 2016

**Abstract.** Palaeoatmospheric records of carbon dioxide and its stable carbon isotope composition ($\delta^{13}$C) obtained from polar ice cores provide important constraints on the natural variability of the carbon cycle. However, the measurements are both analytically challenging and time-consuming; thus only data exist from a limited number of sampling sites and time periods. Additional analytical resources with high analytical precision and throughput are thus desirable to extend the existing datasets. Moreover, consistent measurements derived by independent laboratories and a variety of analytical systems help to further increase confidence in the global $CO_2$ palaeo-reconstructions. Here, we describe our new set-up for simultaneous measurements of atmospheric $CO_2$ mixing ratios and atmospheric $\delta^{13}$C and $\delta^{18}$O-$CO_2$ in air extracted from ice core samples. The centrepiece of the system is a newly designed needle cracker for the mechanical release of air entrapped in ice core samples of 8–13 g operated at −45 °C. The small sample size allows for high resolution and replicate sampling schemes. In our method, $CO_2$ is cryogenically and chromatographically separated from the bulk air and its isotopic composition subsequently determined by continuous flow isotope ratio mass spectrometry (IRMS). In combination with thermal conductivity measurement of the bulk air, the $CO_2$ mixing ratio is calculated. The analytical precision determined from standard air sample measurements over ice is ±1.9 ppm for $CO_2$ and ±0.09 ‰ for $\delta^{13}$C. In a laboratory intercomparison study with CSIRO (Aspendale, Australia), good agreement between $CO_2$ and $\delta^{13}$C results is found for Law Dome ice core samples. Replicate analysis of these samples resulted in a pooled standard deviation of 2.0 ppm for $CO_2$ and 0.11 ‰ for $\delta^{13}$C. These numbers are good, though they are rather conservative estimates of the overall analytical precision achieved for single ice sample measurements. Facilitated by the small sample requirement, replicate measurements are feasible, allowing the method precision to be improved potentially. Further, new analytical approaches are introduced for the accurate correction of the procedural blank and for a consistent detection of measurement outliers, which is based on $\delta^{18}$O-$CO_2$ and the exchange of oxygen between $CO_2$ and the surrounding ice ($H_2O$).

## 1 Introduction

Polar ice cores are unique in providing direct information of the past atmospheric composition. Analysis of entrapped air allows the evolution of the atmospheric composition over the last 800 000 years to be reconstructed (e.g. Lüthi et al., 2008 and references therein; Bereiter et al., 2015). Knowledge of past natural $CO_2$ variations – only several ppm during the Holocene and up to about 100 ppm over glacial/interglacial changes – is crucial to improve predictions of future climate under continued anthropogenic $CO_2$ forcing. Changes in the global carbon cycle fluxes are imprinted in the stable carbon isotope signal of atmospheric $CO_2$ ($\delta^{13}$C, e.g. Köhler et al., 2006). However, carbon isotope measurements of ice core air samples are highly demanding and time-consuming. As a result, detailed measurements of $\delta^{13}$C are still limited to specific time periods (Francey et al., 1999; Indermühle et al.,

1999; Smith et al., 1999; Elsig et al., 2009; Lourantou et al., 2010a, b; Schmitt et al., 2012; Rubino et al., 2013; Schneider et al., 2013; Bauska et al., 2015).

Since the pioneer $CO_2$ measurements in the 1980s (Berner et al., 1980; Delmas et al., 1980; Neftel et al., 1982; Pearman et al., 1986), extraction and measurement techniques have been continuously developed and improved to increase the analytical precision. The initial step of extracting air entrapped in ice is crucial. While extraction of gas by melting the ice is successfully applied for trace gases like $CH_4$, $CO_2$ measurements are generally not reliable in the presence of liquid water (Kawamura et al., 2003). Measurement artefacts arise due to the high solubility of $CO_2$ and chemical reactions of carbonate species in water (Anklin et al., 1995; Zhang et al., 1995; Kawamura et al., 2003). Further challenges arise from adsorption, desorption and contamination effects at surfaces, particularly in connection with mechanical friction between system components (e.g. Zumbrunn et al., 1982), from system leakage, outgassing materials and introduction of contaminants (e.g. drilling fluid). In order to avoid the liquid phase of water, the air must either be extracted in a cooled vacuum chamber by dry mechanical techniques (e.g. Bauska et al., 2014) or by sublimation of the ice matrix (e.g. Schmitt et al., 2011).

When the enclosed air is available in the form of bubbles, the gas extraction efficiency for mechanical systems varies between 60 % and ∼ 90 %. However, in deeper strata where the gas is present in air hydrates (e.g. Uchida et al., 1994) – also called clathrates – extraction efficiencies usually decrease by 10–20 %. For the transition zone, where air bubbles and clathrates coexist, it has been found that $CO_2$ is enriched in clathrates and depleted in air bubbles. In this zone, measurements of $CO_2$ mixing ratios can thus be severely biased as they depend on the gas extraction efficiency (Ikeda et al., 1999; Sowers and Jubenville, 2000; Ahn et al., 2009; Schaefer et al., 2011; Bereiter et al., 2014). At the cost of a slow extraction process which limits sample throughput, this problem can be avoided by sublimation of the ice matrix, resulting in close to 100 % extraction efficiency (Güllük et al., 1998; Schmitt et al., 2011). Anyhow, while measurements of $CO_2$ mixing ratios by mechanical extraction systems are affected in the transition zone from bubble to clathrate ice, only a decrease in precision but no systematic effect could be observed for $\delta^{13}C$ analysis of $CO_2$ (Schaefer et al., 2011 and references therein). In addition, for pure bubbly ice, the extraction efficiency is not a concern for $CO_2$ measurements and no difference has been observed compared to results derived by sublimation systems.

A variety of mechanical extraction systems are in use. In a needle cracker (NC), the ice is crushed to small pieces and air is released from the thereby opened bubbles (Zumbrunn et al., 1982). The system described by Bereiter et al. (2013) pulverizes ice samples by continuously shaving off thin layers of the sample surface by a centrifugal ice microtome (CIM). Alternatively, ice samples are ground in a ball mill when both the ice sample and stainless steel balls inside a small container are shaken (Barnola et al., 1995; Lourantou, 2009), or grated into small chips by shaking the ice in a vessel containing a perforated inner cylinder ("cheese grater", Etheridge et al., 1996).

Only a few laboratories have the ability to do ice core analysis of both $CO_2$ concentrations and its stable isotopic composition. In the following, the published and recently operated analytical systems allowing measurements of both parameters on a single ice sample are summarized (see Table 1 for detailed system characteristics). All systems use isotopic ratio mass spectrometry (IRMS) to detect the different mass ratios between the stable $CO_2$ isotopologues ($m/z$ 44, 45 and 46).

The Laboratory of Climate and Environmental Physics (KUP, Bern, Switzerland) operates two such systems. For the mechanical extraction system (NC) the released air is first expanded over a water trap into a small volume where the gas pressure is measured for evaluation of the $CO_2$ mixing ratio in combination with the IRMS signal. Using helium as a carrier gas, the gas sample is then flushed into a preconcentration system (PreCon) to separate the main components of air. In order to avoid isobaric interference, $CO_2$ is separated from $N_2O$ and organic compounds (e.g. from drilling fluids) by gas chromatography (GC) before being injected into the IRMS via an open-split interface (Elsig et al., 2009). In the sublimation system, sublimated water is quantitatively removed before the liberated air is cryogenically collected. Then, the basic principle is similar to the system described before but extraction and GC–IRMS are decoupled (Schmitt et al., 2011). KUP additionally operates one system (CIM) solely dedicated to the analysis of the $CO_2$ mixing ratio (Bereiter et al., 2013), which replaces their initial NC system described by Zumbrunn et al. (1982) and modified by Lüthi (2009).

The Laboratoire de Glaciologie et Géophysique de l' Environnement (LGGE, Grenoble, France) uses a ball mill for mechanical extraction before the air is directly released to the inlet system of a coupled GC–IRMS for $CO_2$ mixing ratio and $CO_2$ stable isotope analysis (Barnola et al., 1995; Lourantou, 2009).

The ice core and quaternary geochemistry lab at Oregon State University (OSU, USA) also uses a mechanical extraction system (cheese grater). A small aliquot of the extracted sample gas is isolated from the grater and finally trapped at −260 °C after water is removed at −100 °C. The $CO_2$ mixing ratio is then determined by GC. The rest of the gas, again first passing a water trap at −100 °C, is condensed in a second trap at −190 °C and finally analysed for $\delta^{13}C$ by IRMS dual-inlet measurement, applying a correction for the isobaric $N_2O$ interference. Interference from drilling fluid contamination can potentially be a problem for certain samples. The rather large sample size allows measurement of $N_2O$ in addition (Bauska et al., 2014). OSU also operates a NC system for the analysis of $CO_2$ only (Ahn et al., 2009).

**Table 1.** Characteristics of published and recently operated analytical systems allowing measurement of $CO_2$ mixing ratios and the $CO_2$ stable isotopic composition on a single ice sample. Indicated precisions ($1\sigma$) are estimated from replicate analysis of natural ice samples. One should note that the thereby applied metric may not be entirely comparable (e.g. replicates either measured on different or on the same day).

| Laboratory | Extraction principle (design) | Operating temp. (°C) | Sample mass (g) | Extraction efficiency for bubbly (clathrate) ice | Daily sample throughput | Precision $CO_2$ (ppm) | Precision $\delta^{13}C$ (‰) |
|---|---|---|---|---|---|---|---|
| KUP | mechanical (NC) | −20 (−35)* | 5–6 | ∼ 70 (∼ 50) % | 3–6 | 2.0 | 0.07 |
| | sublimation | | ∼ 30 | ∼ 100 (∼ 100) % | 1–2 | ∼ 2.0 | 0.05 |
| LGGE | mechanical (ball mill) | −65 | 40–50 | ∼ 70 (not reported) % | 1–2 | 1.5 | 0.1 |
| OSU | mechanical (cheese grater) | −60 | 400–550 | ∼ 60 (< 60) % | 1–2 | 1.9 | 0.02 |
| CSIRO | mechanical (cheese grater) | −20 | 800–1000 | 60–80 (unknown) % | 3–4 | 1.0 | 0.04 |
| CIC (this study) | mechanical (NC) | −45 | 8–13 | 70–80 (∼ 60) % | 3–4 | 2.0 | 0.11 |

* Initially reported at −20 °C, but lowered to −35 °C since (Leuenberger, 2009).

CSIRO uses a cheese grater for mechanical extraction (Etheridge et al., 1996; MacFarling Meure et al., 2006; Rubino et al., 2013). The released air is cryogenically collected in an external trap (around −260 °C) after removing water at −100 °C. Subsequently, the sample is analysed using GC for determination of the $CO_2$ mixing ratio and by IRMS for $\delta^{13}C$ without further GC separation and purification. A correction for the isobaric $N_2O$ interference is applied. Interference from drilling fluid contamination can potentially be a problem for certain samples. The large sample size allows measurement of other trace gases from the same sample ($CH_4$, CO, and $N_2O$).

In this study, we present a new system built at the Centre for Ice and Climate (CIC, University of Copenhagen, Denmark) in the laboratory for atmospheric trace gas measurements in ice cores (Stowasser et al., 2012; Sperlich et al., 2013). The approach was to opt for small sample size, to allow simultaneous analysis of both $CO_2$ mixing ratios and its stable isotopic composition in the same sample, and to achieve high precision with reasonable throughput in order to pursue high resolution sampling schemes. We thereby followed the extraction principle of the NC using a modified design. Due to the intended small sample size, the extraction unit was coupled to a continuous flow GC–IRMS set-up, with the benefit of overcoming the problem of interference from isobaric $N_2O$ and fragments of remaining contamination from drilling fluid.

## 2 Instrumental set-up and standards

### 2.1 Dry extraction unit

The dry extraction unit was designed based on the NC principle for small sample sizes of a few grams described by e.g. Lüthi (2009) and Ahn et al. (2009). However, some major modifications were implemented to achieve the following goals: (i) avoidance of mechanical friction within the system in order to reduce related contamination and adsorption/desorption effects (Zumbrunn et al., 1982; Stauffer et al., 1985; Lüthi, 2009); (ii) operation at very low temperatures to reduce the risk of $CO_2$ in situ production (within the extraction unit) from chemical reactions due to the presence of $H_2O$ in the mobile phase; (iii) fast and simplified sample loading with minimal exposure of inner surfaces to ambient air in order to maximize sample throughput and to reduce artefacts from surface effects, respectively.

Our NC design for ice samples with maximum dimensions of $2.3 \times 2.5 \times 2.5\,cm^3$ and a typical mass of 8–13 g is shown in Fig. 1. All inner parts are made from stainless steel (SS). Similar to Ahn et al. (2009), we use a compressible welded bellow (SS, Comvat, Germany, 5 in Fig. 1). This allows crushing of the ice by axial movement of the needles mounted with a hot/cold press fit (hardened SS, 1.5 mm OD, 30 mm length, Dema, Germany, 6 in Fig. 1). In comparison to the design described by Lüthi (2009), which requires a vacuum tight seal around a movable piston, the mechanical friction within our unit is thus strongly reduced. In addition, the bellow is mounted differently than in the design presented by Ahn et al. (2009), resulting in an inner volume of half the size ($\sim 110\,cm^3$; $\sim 63\,cm^3$ with the bellow compressed) and an inner surface area reduced by about two-thirds. A small volume is favourable in terms of evacuation speed and time required for transferring the gas out of the extraction unit for subsequent treatment. A small inner surface reduces the potential for surface effects (adsorption/desorption) which can bias the $CO_2$ stable isotope ratios due to isotopic fractionation processes. The extraction unit is connected to the rest of the set-up by 1/4 in. SS tubes welded to the NC and equipped with valves (SS–4H, Swagelok, USA, 11, 12 and

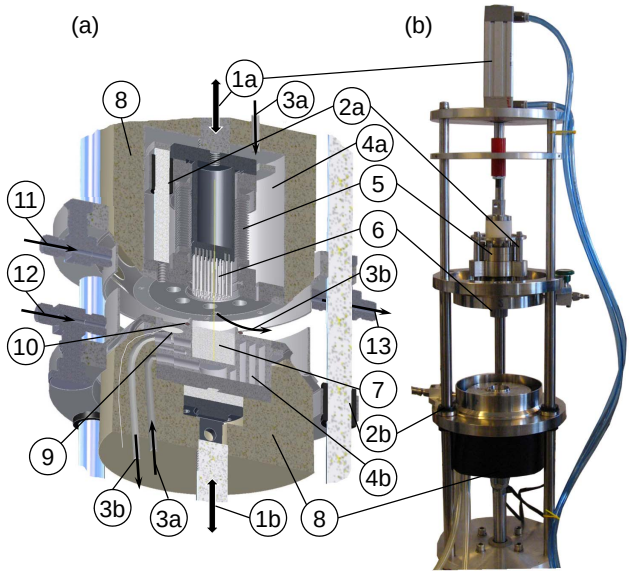


**Figure 1. (a)** Schematic of the CIC needle cracker (NC) dry extraction unit and **(b)** picture with cooling jacket and insulation dismounted at the top part. Pneumatic actuators (1a, 1b), guiding SS rods with bearings (2a, 2b), cold air inlet and outlet for cooling (3a and 3b respectively), cooling jacket and cooling cavities (4a and 4b, respectively), SS welded bellow (5), SS needle pins (6), ice sample (7), insulation (8), temperature sensor (9), indium wire for vacuum seal (10), gas inlets (11, 12) and outlet (13) equipped with valves.

13 in Fig. 1). A fixed soft copper seal connects the needle piston to the bellow base plate.

Both the crushing mechanism by axial compression of the bellow and the opening/closing mechanism are pneumatically actuated. To crush the ice sample, a pressure of 4.7 bar is applied to the upper cylinder (CP95SDB40–80, SMC, 1a in Fig. 1) and the needles are actuated via a 5-port solenoid valve (VQZ3120–5YZB–C10, SMC) controlled by an external logical device (homemade). The total number and frequency of strokes can be controlled and were typically set to 37 and $\sim 3$ Hz, respectively. Six bars of air pressure applied on the lower actuator (C95NDB80–250, SMC, 1b in Fig. 1) creates enough force for a vacuum tight sealing between the connection of the upper and lower part of the extraction unit using indium wire (1.5 mm OD, 99.99 %, Sigma-Aldrich, USA, 10 in Fig. 1). Although the wire needs to be replaced whenever a new sample is loaded, the indium can be reused when drawn into wire again. This sealing mechanism reduces the amount of time required to open and vacuum seal the vessel compared to systems using bolts and nuts. It takes less than 2 min, including the removal of previously crushed ice, cleaning and reloading of a new sample. To minimize contact of ambient air with the inner surfaces and avoid condensation/deposition of water vapour, both the lower and upper part of the device are flushed through the respective inlets with $N_2$ (99.999 %, Air Liquid, Denmark) whenever the system is opened.

To cool the well-insulated NC, we chose to use an air cooling set-up similar to that described by Schmitt (2006) instead of using a liquid cooling fluid. Pressurized air with an adjustable flow between 0 and $\sim 60\,\mathrm{L\,min^{-1}}$ is dried in two sequential traps (filled with Molecular sieve 13X/4Å, Supelco, USA) and cooled in a copper heat exchanger mounted in a Dewar (D2). D2 is supplied with droplets of liquid nitrogen (LN) from a larger Dewar (D1) containing the LN reservoir. The droplets are pumped by applying 12.8 V to a heater (10Ω resistor) mounted in the widened inlet of an empty 1/4 in. tube submerged in the LN. Whenever heat is applied, LN evaporates around the heater and the evolving $N_2$ bubbles transport the above, still liquid nitrogen through the isolated tube to D2. This LN pump is regulated by the use of two coupled proportional–integral–derivative controllers (PID, iTRON 08, JUMO, UK). One PID is set to the desired final temperature measured in the NC (9 in Fig. 1), whereas the other is set to a minimum temperature of −180 °C in D2, preventing the system from eventual clogging by frozen remnant water in the air stream and from potential condensation of oxygen. The temperatures used for PID input and survey of the air stream are measured with platinum resistance thermometer PT100 elements (100Ω, −200 to 600 °C, Class 1/10, TC Direct, USA). By changing the settings for air flow and/or the set points for NC and D2, the air stream temperature is regulated. To cool the NC, the cold air stream is split in front of the unit and either directed through the cavities in the lower part of the massive steel unit (4b in Fig. 1) or the cooling jacket mounted around the compressible welded bellow (4a in Fig. 1). The minimum operating temperature of the NC is −55 °C, whereas the standard operating temperature is set to −45 °C (stability ±1 °C) with significantly reduced build-up of ice on the vacuum sealing surfaces. While cooling down to −45 °C, the air stream first regulates to about −80 °C before it stabilizes at −60 °C. Cooling the NC to −45 °C takes around 70 min.

Compared to other systems allowing analysis of similarly small sample sizes (other NC designs, CIM) the operating temperature of our extraction chamber is significantly lower (−45 °C compared to around −35/−30 °C). This is beneficiary because the resulting lower water partial pressure in the extraction chamber (about 5-fold) reduces the risk of in situ $CO_2$ production by wet chemistry. This is supported by the findings of Bauska et al. (2014) which indicated that operating at low temperatures improves precision and decreases the blank of the method. For our design this is reflected in a reduced system offset compared to the KUP NC (Sect. 4.1.1), though most likely resulting from a combined positive effect of friction-reduced motion and lower operating temperature. The low water vapour partial pressure allowed a water trap to be omitted at the exit of the extraction unit.

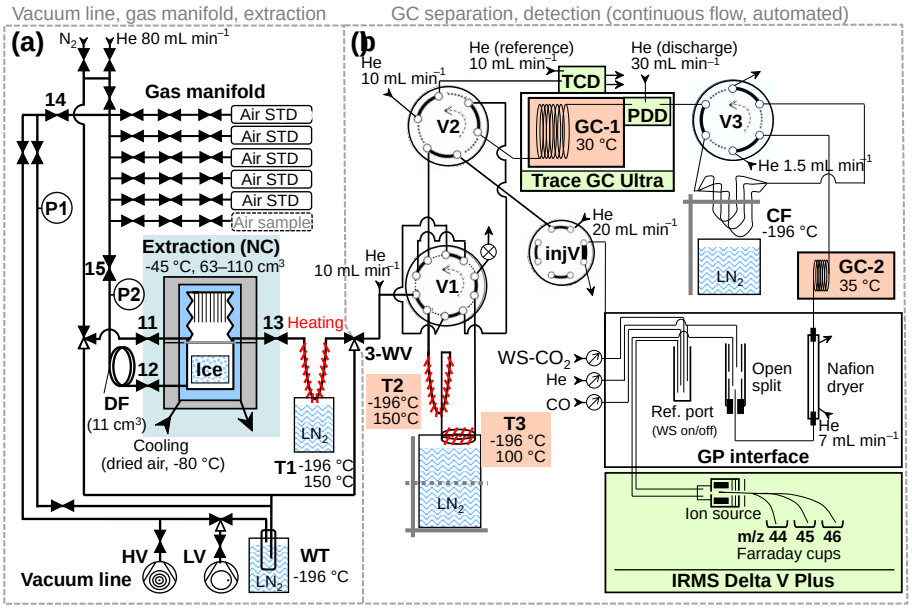


**Figure 2.** Schematic representation of the new analytical CIC system for simultaneous measurements of $CO_2$ mixing and stable isotope ratios. The set-up consists of a manually operated section A, allowing injection and loading of air and ice samples, and a fully automated section B, for gas separation, purification and final detection run in continuous flow mode. Highlighted in red and green are components for gas separation and detection, respectively. See main text for details (Sects. 2 and 3).

### 2.2 Analytical system

Our analytical system allows simultaneous measurements of atmospheric $CO_2$ mixing ratios and its stable isotopic composition in the same sample. A schematic representation of the system is shown in Fig. 2. It can be divided into two main sections: section A (manually operated) for standard or sample gas loading, and section B (fully automated and in continuous flow mode) for gas separation (PreCon) and injection into the detection systems.

Section A consists of four main parts:

i. a vacuum line;

ii. a gas manifold for carrier-, protection- or standard-gas injection;

iii. a dry extraction unit (NC);

iv. a trap (T1) to quantitatively cryopump sampled gas out of the NC for subsequent and complete transfer from section A to B.

Section B consists of two main parts:

i. a gas separation part which allows initial trapping of the transferred sample (T2), separation of $CO_2$ (and $N_2O$) from the major air components (T3) and subsequent partitioning of the two fractions to individual lines for either final detection (main air fraction) or further purification by gas chromatography (GC–1 and GC–2);

ii. the detection systems including a thermal conductivity detector to quantify the amount of the main air fraction (TCD, VICI, USA, integral part of GC–1, TRACE GC Ultra, Thermo Scientific, USA), a pulsed discharge detector to survey $CO_2$ separation and purification (PDD, VICI, USA, integral part of GC–1) and an IRMS to quantify amount and isotopic ratios of the $CO_2$ fraction (Delta V Plus, Thermo Fisher, Germany).

All inner surfaces of the set-up are either made from SS or fused silica and the connections are either welded or sealed with metal or graphite/vespel ferrules to exclude artefacts due to outgassing (Sturm et al., 2004). Section A can either be evacuated or flushed with $N_2$ (inert gas also used for protection of inner surfaces when the extraction unit is opened) or He (99.9995 %, Air Liquide, Denmark) additionally purified by a getter (Gas Purifier, VICI, Valco Instruments Co. Inc, USA). Similar to the gas manifold, the vacuum line is made from 1/4 in. SS tubes and equipped with on/off valves (SS–4H, Swagelok, USA). It includes a low vacuum (LV) rotary vane pump (EDM2, Edwards, UK) and a turbo pump (TMU 071, Pfeiffer, Germany) to reach high vacuum (HV). The LV pump is used for the fast removal of large quantities of gas (e.g. after sample loading) and is protected from the analytical line by a liquid nitrogen trap (WT). All lines in section B are always above atmospheric pressure and continuously flushed with He used as a carrier gas for the entire system, allowing transfer of sample/standard gas from the extraction unit to the detection systems which are all run in continuous flow mode. Further details will be given in Sect. 3.

**Table 2.** CIC reference standards for $CO_2$ mixing and stable isotope ratios.

| Name | Reference | Gas | $CO_2$ (ppm) | $\delta^{13}$C-$CO_2$ (‰ VPDB) | $\delta^{18}$O-$CO_2$ (‰ VPDB-$CO_2$) |
|---|---|---|---|---|---|
| Messer–649250[1] | GS19/GS20 | $CO_2$ | | $-6.004 \pm 0.008$ | $-10.80 \pm 0.13$ |
| CA08274[2,3] | NOAA/CIC | Air | $181.04 \pm 0.06$ | $(-35)^*$ | $(-32)^*$ |
| CA08054[2,4] | NOAA | Air | $267.08 \pm 0.01$ | $-7.779 \pm 0.002$ | $-7.531 \pm 0.005$ |
| CA08292[2,3] | NOAA/CIC | Air | $400.53 \pm 0.02$ | $(-35)^*$ | $(-31)^*$ |
| AL-1[3,5] | CIC | Air | $215.8 \pm 0.7$ | $-9.26 \pm 0.04$ | $-8.02 \pm 0.07$ |
| AL-2[3,5] | CIC | Air | $368.9 \pm 0.5$ | $-9.80 \pm 0.02$ | $-9.73 \pm 0.08$ |
| NEEM–2[3,5] | CIC | Air | $378.6 \pm 0.5$ | $-8.0 \pm 0.1$ | $0.1 \pm 0.1$ |

[1] Stable isotopic composition calibrated at CIC by IRMS dual-inlet against GS19 and GS20 (Centre for Isotope Research, Gröningen University, Netherlands). [2] $CO_2$ mixing ratio calibrated and certified by NOAA ESRL/GMD (Boulder, Colorado, USA). [3] Stable isotopic composition calibrated at CIC against Messer–649250 and CA08054 with the set-up described in this study but in "dry mode" (without ice). [4] Stable isotopic composition calibrated by the Stable Isotope Lab at INSTAAR (SIOL, University of Colorado, USA) in cooperation with NOAA. [5] $CO_2$ mixing ratio calibrated at CIC against the three NOAA standards CA08274, CA08054 and CA08292, with the set-up described in this study and by WS-CRD spectroscopy. * Values outside of the reliable calibration range.

### 2.3 Standards

The reported $CO_2$ mixing ratios (also referred to as $CO_2$ concentrations in the literature) are defined as the dry air mole fraction expressed in parts per million by volume (ppm), and are linked to the World Meteorological Organization (WMO) mole fraction scale for $CO_2$ in air (Tans and Zhao, 2003; Zhao and Tans, 2006). Isotope ratios are reported relative to the international measurement standards (VPDB, VPDB-$CO_2$ and VSMOW for $^{13}$C-$CO_2$, $^{18}$O-$CO_2$ and $^{18}$O-$H_2O$, respectively) using the delta notation:

$$\delta = \left( \frac{R_{\text{sample}}}{R_{\text{standard}}} \right) - 1, \quad (1)$$

where $R$ denotes the ratio of the heavy to light isotope in the sample and the standard, respectively. Our working standards were selected in order to cover the range of atmospheric $CO_2$ mixing and stable isotope ratios expected for glacial to interglacial conditions (Table 2). With these standards, system characterization, daily calibration and continuous quality control sample (QCS) measurements were performed (Sects. 3 and 4).

For referencing IRMS measurements, a working standard (WS) of pure $CO_2$ from a natural source (Messer–649250, Messer, Italy) is injected via an open-split interface (GP interface). Its stable isotopic composition was referenced at CIC against pure $CO_2$ reference gases GS19 and GS20 from the Centre for Isotope Research (Gröningen University, Netherlands; Meijer, 1995) by IRMS dual-inlet measurement (Delta V Plus, Thermo Fisher, Germany). For air standards we used three synthetic air mixtures, in the following called CA08274, CA08054 and CA08292 provided by the Global Monitoring Division of the Earth System Research Laboratory at the National Oceanic and Atmospheric Administration (NOAA ESRL/GMD, Boulder, USA), two pressurized air tanks called AL-1 and AL-2 (Air Liquid, Denmark) and one of two atmospheric air tanks sampled in 2008 at a clean-air site of the NEEM deep ice core drilling camp called NEEM–2. The three NOAA tanks have been calibrated and certified by the NOAA ESRL/GMD Carbon Cycle Gases Group for $CO_2$ mixing ratios. The other tanks have then been calibrated against these three standards at CIC both with the set-up described in this study and directly from the tanks by wavelength-scanned cavity ring-down spectroscopy (WS-CRDS; CFADS36 $CO_2$/$CH_4$/$H_2O$ analyser, Picarro Inc., USA). The stable isotopic composition of CA08054 has been calibrated by the Stable Isotope Lab at INSTAAR (SIOL, University of Colorado) in cooperation with the NOAA Climate Monitoring and Diagnostics division (CMDL). The stable isotopic composition of the two other NOAA cylinders and of AL-1, AL-2 and NEEM-2 has been calibrated at CIC against Messer–649250 and CA08054 with the set-up described here. All tanks were equipped with high-purity regulators (Y13–C444A, single stage, stainless steel with Kel–F and Teflon seals, Airgas, USA).

## 3 Measurement procedures and quality control

### 3.1 PreCon system

The pure $CO_2$-WS (Messer–649250) is injected via an open-split interface (GP interface) for referencing of IRMS measurements but can optionally also be passed through the automated section B of the system (Sect. 2.3, Fig. 2). This allows the assessment of potential fractionation effects from gas trapping and GC separation (Sect. 4.1.2). In the daily routine this is useful for an immediate control of conditions and stability of the PreCon, GC and detection systems. At the beginning of each measurement day, such injection runs, variable in the amount as well as blank runs for this part of the set-up, were therefore analysed (Table 3).

**Table 3.** Example of a daily measurement sequence. See Table 2 for details on standard gases (WS, air standard) and the main text for analytical procedures. BFI denotes bubble-free ice.

| Daily run | Type of sample | Sample name | Comment | Set-up[1] | Data processing[2] |
|---|---|---|---|---|---|
| 1 | WS – 0.4 µL | Messer–649250 | first run of the day | B | (discard) |
| 2 | Blank | Blank | | B | determination/control of blank |
| 3 | WS – 0.4 µL | Messer–649250 | first run after blank | B | (discard) |
| 4 | WS – 0.2 µL | Messer–649250 | | B | control of day-to-day stability, |
| 5 | WS – 0.4 µL | Messer–649250 | | B | drift and size dependency |
| 6 | Air standard | CA08054 | sample loaded – NC opened | A, B | (discard, NC surface effects) |
| 7 | Air standard | CA08054 | | A, B | (discard) |
| 8 | Air standard | CA08054 | | A, B | daily calibration & drift correction |
| 9 | ICE | DE08–439 | ice crushed | A, B | RESULT |
| 10 | Air standard | CA08054 | | A, B | daily calibration & drift correction |
| 11 | Air standard | CA08054 | sample loaded – NC opened | A, B | (discard, NC surface effects) |
| 12 | ICE | GRIP 250–12 | ice crushed | A, B | RESULT |
| (12)[3] | BFI | BFI (w or w/o CA08054) | BFI crushed (or not crushed) | A, B | procedural blank |
| 13 | Air standard | CA08054 | | A, B | daily calibration & drift correction |
| 14 | Air standard | CA08054 | sample loaded – NC opened | A, B | (discard, NC surface effects) |
| 15 | ICE | DE08–443 | ice crushed | A, B | RESULT |
| 16 | Air standard | AL-2 | | A, B | daily calibration |
| 17 | Air standard | AL-1 (AL-2)[3] | | A, B | quality control sample (QCS) |
| 18 | Air standard | CA08054 | sample loaded – NC opened | A, B | (discard, NC surface effects) |
| 19 | ICE | DE08–426 | ice crushed | A, B | RESULT |
| 20 | Air standard | CA08054 | | A, B | daily calibration & drift correction |
| 21 | Air standard | AL-1 (CA08292/CA08274)[3] | | A, B | daily calibration |
| (21)[3] | Air standard | CA08054 | different injection size | A, B | control of size independency |

[1] Section of system passed by the analysed gas sample (see Fig. 2). [2] See main text for details about data processing. [3] Alternative measurement option.

The following step by step description of the measurement procedure follows part numbering and abbreviations as indicated in Fig. 2. Connected in series, the cryogenic traps T2 (1/4 in. SS Swagelok tube, filled with around 5 cm of HayeSep D, 100/120 mesh, Sigma-Aldrich, Switzerland) and T3 (empty 1/16 in. SS Swagelok tube) are cooled by being immersed into liquid nitrogen. In order to prevent ambient air to be sucked into these traps while cooling down, the on/off valve (SS–4BK–TW–1C, Swagelok, USA) at the vent is closed. Then, various amounts of pure $CO_2$-WS are injected directly onto T2 with valve V1 (10-port, 1/8 in., air actuated, A210UWM, VICI, USA) switched compared to Fig. 2. To vary the injected amount an internal sample injection valve with a defined volume of 0.1 µL is switched for the selected number of times (injV, AN14WM.1, VICI, USA). Alternatively, if the valve is not switched, only helium carrier gas is passed through the system (20 mL min$^{-1}$, set by a flow controller, Model VCD 1000, Porter, USA) and a blank measurement for this section of the system is obtained. In any case, V2 (6-port, 5UWM, VICI, USA) is switched after a trapping time of 6 min – similar to the trapping time applied for air standard and ice sample measurements – directing the sample gas flow (10 mL min$^{-1}$ set by a flow controller; VCD 1000, Porter, USA) through the TCD detector. After an idle time of 30 s allowing the flow to stabilize, the LN Dewar cooling T2 and T3 is automatically lowered by a double activated pneumatic cylinder (CD85N20–250B, SMC, Denmark) to a level at which T3 is still cooled. T2 is then heated by a rope heater (FGR–060, Omegalux, UK) to the set temperature of 150 °C regulated by a PID controller (iTRON 08, JUMO, UK). Thereby, the trapped gas is released and the amount of the main air components is detected by the TCD (no signal for pure $CO_2$ and for blanks) while both $CO_2$ and $N_2O$ are trapped in T3 for later separation and detection in a second line (typical chromatograms for measurements of $CO_2$-WS, procedural blanks and ice core samples can be found in Supplement Figs. S1 and S2 and in Fig. 3, respectively). After 5 min, V2 is switched again, now redirecting the sample flow (again 20 mL min$^{-1}$) through this alternative detection line. After an idle time of 40 s allowing the flow to stabilize, the LN Dewar is further lowered and trap T3 quickly heated to 100 °C (resistance wire, 2.5Ω m$^{-1}$, 5 m, Conrad Electronics, Germany) regulated by a second PID controller (iTRON 32, JUMO, UK). Thereby, $CO_2$ and $N_2O$ (not present in the pure $CO_2$-WS) are released and the different gases are subsequently separated by the gas chromatographic fused silica capillary column in the GC–1 (30 °C, CP–PoraBond–Q, 25 m × 0.53 mm ID, d$f$ = 10 µm, Varian,

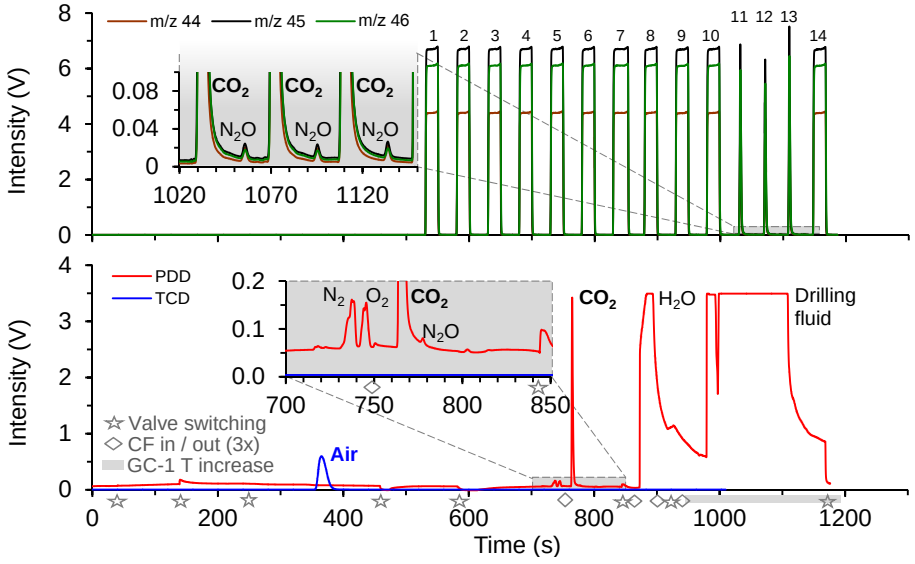


**Figure 3.** Chromatograms for the measurement of an ice sample as described in Sect. 3.2. Upper panel: IRMS signal intensity for $m/z$ 44, 45 and 46. Injections of the WS via the open split are identifiable by the flat-topped peaks. Peaks 1–9 are used to reach stable source conditions while peaks 10 and 14 before and after the samples are used for referencing. The inset shows baseline details and $N_2O$ separation in detail. Lower panel: PDD and TCD intensity signal for $CO_2$ and air, respectively. Stars indicate valve switching, resulting in small variations in the PDD signal due to changes in pressure and flow (see inset, not detected by the less sensitive TCD). Diamonds indicate immersion of the three capillary traps into liquid nitrogen for $CO_2$ cryofocusing and their subsequent one-by-one release resulting in the three peaks of the split sample shown in the upper panel (peaks 11–13). Over the time period, indicated by the grey bar, the GC–1 temperature is increased to 150 °C in order to precondition the column for the next sample (release of water and remnants of drilling fluid contamination). The enlargement shows baseline details revealing the $N_2O$ peak and small remains of $N_2$ and $O_2$ from the air sample, incompletely separated by the preceding cryogenic partition.

USA). The signal then being detected by the PDD is shown in Fig. S1 (Supplement). Shortly before the eluted $CO_2$ peak arrives at the PDD (discharge gas flow set to 30 mL min$^{-1}$), three parallel traps (fused silica capillaries, 250 µm ID, 1.8 m length, BGB, Germany) are immersed into LN to re-trap $CO_2$ and $N_2O$ for cryogenic focus (CF) after splitting the sample stream at the PDD outlet valve V3 (GC built in 6-port valve, VICI, USA). To vent remaining $H_2O$ and potential contaminants from drilling fluid (for ice samples), V3 is switched before the signal is detected in the PDD ($\sim$ 70 s after the maximum in the $CO_2$ peak). The GC column is then conditioned for the next sample by heating to 150 °C. In the separated part of the line, the three CF capillaries are meanwhile lifted one after the other out of the LN, subsequently releasing the sample – now split in three aliquots – for further transport in a reduced He flow of 1.5 mL min$^{-1}$. To avoid isobaric interference, $CO_2$ and $N_2O$ contained in these aliquots are again separated in a second GC column (GC–2; 35 °C, CP–PoraBond–Q, 40 cm × 0.53 mm ID, d$f$ = 10 µm, Varian, USA) before the remnant water vapour is removed by a Nafion drying column (40 cm × 0.36 mm ID , Perma Pure Inc., USA). Finally, the sample gases are introduced to the IRMS via the open split of the GP interface. Before the three $CO_2$ sample peaks elute, the reference gas ($CO_2$-WS, here the same as the sample gas) is injected several times (reference port) in order to reach stable IRMS-source conditions. The peak amplitude is thereby adjusted to closely match the amplitude of the sample aliquots (not for blanks). For the same reason a constant CO background flow through the reference open-split port into the ion source was maintained as proposed in Elsig and Leuenberger (2010). The mean value of the peak before and after the sample is ultimately used for referencing. Splitting the sample in aliquots allows for three IRMS measurements on the same sample theoretically improving the analytical precision. In practice, the therefore required quantitative splitting in three evenly sized aliquots is difficult to achieve. For the calculated mean values (weighted by mass, i.e. size) no difference in final precision compared to a single measurement was observed. However, results from these multiple measurements could be statistically analysed and were useful, e.g., to evaluate the applied IRMS nonlinearity correction which reduces the standard deviation over the three replicates (Sect. 4.1.2).

The total measurement time from injection to final IRMS detection is 21 min. It is longer for air standard and ice sample measurements, as these include section A of the system (Sect. 3.2).

### 3.2 Standard air, ice samples and blanks

Air standards and blank measurements were performed regularly for calibration and system characterization, thereby following the exact procedure used to measure real (natural) ice samples, i.e. following the "identical treatment" principle (Werner and Brand, 2001). To simulate the entire measurement procedure as close as possible, artificial bubble-free ice (BFI) samples were used. BFI was produced from ultrapure water (MilliQ, 18.2MΩ cm at 25 °C) degassed for 60–90 min using a roughing LV pump (E2M0.7, Edwards, UK) and then slowly frozen from the bottom (20 cm in 48 h), thereby forcing the remaining gas out of the water. Results for calibrations and system characterization will be presented in Sect. 4.

Samples of air, either from tanks (e.g. atmospheric samples or standards) or extracted from ice core samples, pass all sections of the experimental set-up (A and B, Fig. 2). When the system is not in use (e.g. overnight), section B is constantly flushed with He while all lines in section A and the NC are pressurized slightly above atmospheric pressure with He and $N_2$, respectively. Prior to analysis, ice core or BFI samples are cut to the required dimensions and the surfaces are decontaminated by removing the top layers with a scalpel.

A typical daily measurement sequence is listed in Table 3. The measurements can be separated into five main categories:

1. air standard measurements performed by injecting variable amounts of the standard gas over an ice sample of either natural or artificial origin (BFI) without crushing the ice; standards of different $CO_2$ mixing ratios and isotopic composition were thereby used (Table 2);

2. system blank measurements performed by omitting addition of standard gas and hence resulting in sampling carrier gas only;

3. BFI measurements either performed with air standard added or omitted but with the ice being crushed;

4. measurements simulating the crushing procedure (i.e. needles moved) but using BFI which has been crushed in advance; in this case, artefacts from remnant gas potentially present in the initial, intact BFI sample can be excluded (Sect. 4); these measurements were also performed with and without the addition of air standard; the latter case will be further referred to as "procedural blank";

5. measurements of air extracted from natural ice samples by crushing the ice.

The following step by step description of the measurement procedure follows part numbering and abbreviations as indicated in Fig. 2. Section A and the NC are prepared for measurements during the first five runs of the daily sequence (Table 3). The procedure for these runs is described in Sect. 3.1. After the air cooling system of the NC is started, the first ice sample is loaded once a temperature of −20 °C has been reached. While the unit is open, both the upper and lower parts are continuously flushed with $N_2$ through the respective inlets (11 and 12) to prevent contamination from ambient air and condensation of water vapour on the cold inner surfaces. After the NC is closed and vacuum sealed again, inlets 11 and 12 are closed and the $N_2$ flow is turned off.

Each time the NC is opened, the following sequence of steps is required for evacuation and reconditioning. The chamber is evacuated by the LV pump through inlet 11 for 1 min. Only port 11 is used in this evacuation step to prevent trapping of $N_2$ on trap T1 (heated to 100 °C, 1/4 in. SS tube, filled with HayeSep D, 100/120 mesh, Sigma-Aldrich). This is essential because at this point the $N_2$ abundance in the NC is much higher than in samples of recent or past atmosphere. When the system is evacuated, inlet 12 remains always closed. To avoid analytical artefacts, this inlet is only used with a one-directional flow into the NC, thus preventing water vapour from reaching the gas manifold and the vacuum lines used for the injection of standard air samples. When the pressure in the NC has dropped, trap T1 and the rest of the vacuum lines still filled with He or $N_2$, respectively, are now also evacuated through the respective lines. After a few seconds the vacuum system is switched to the HV pump for another 5 min. To precondition the NC, the chamber is closed off from the vacuum (valves 11 and 13) and then filled with an aliquot of air standard through inlet 12. Since the standard added in this step is used only for conditioning, the injected amount is non-quantitative. After inlet 12 is closed again, T1 is cooled down by being immersed in LN before outlet 13 is opened to cryogenically pump the air aliquot onto T1. After a trapping time of 3 min, the line (vacuum line–NC–T1) is flushed with He from the inlet next to the gas manifold set to a flow of 80 mL $min^{-1}$ (gas flow controller, Model 100, VICI, USA). Since this air aliquot is not to be analysed, the He gas flow is then directed through the 3-way valve (3-WV; SS–43GXS4, Swagelok, USA) into the LV pump. To release the previously trapped air sample while flushing, T1 is heated by a rope heater (FGR–060, Omegalux, UK) to the set temperature of 150 °C regulated by a PID controller (N2300, West Instruments, USA). After a flushing time of 3 min, outlet 13 and inlet 12 are closed and the temperature of T1 is reduced to 100 °C. The system is now in a similar state as prior to runs where the NC has not been opened beforehand (see Table 3).

To start an acquisition run, the NC, T1 and all vacuum lines are evacuated for ∼ 10 min until reaching a pressure of $2 \times 10^{-3}$ mbar monitored by P1 (Single Gauge Pirani Transmitter, Pfeiffer, Germany; in a dry system, a vacuum $< 5 \times 10^{-4}$ mbar, the lower detection limit of P1 is reached). The gas manifold allows selection between the different air standards (Air STD) and the amount to be injected. For this purpose, gas can be expanded into a defined volume adjustable in size by the valves included in each line. For each

expansion step, an equilibrium time of 2 min was applied. In every sequence, the first run which includes section A (run 6) is performed using an air standard of large size (aliquot expanded from the volume between the first and last valves of the gas manifold line). This allows for a first immediate control of system conditions and day by day stability after the idle time overnight. From the gas manifold the sample is expanded into a defined volume of $\sim 11\,cm^3$ (DF), equipped with another pressure gauge, P2 (high-precision piezo pressure transmitter, PAA–35X, Keller AG, Switzerland). After DF has been closed off towards the manifold (valve 15) and the NC (inlet 12 has been closed initially), the pressure is recorded for later use (Sect. 4.1.1). At the same time, sample air contained in the rest of the lines is pumped off by the HV pump. After the pressure has been recorded and valves 11 and 13 have been closed, the gas is further expanded into the NC. The standard gas is kept in the NC for 2 min, simulating the procedure applied for natural ice samples which are crushed at this point, allowing the gas to subsequently expand from the ice. The valve to DF is thereby kept open, which allows us to record and survey the efficiency of gas extraction from the opened bubbles when measuring natural ice samples and subsequently the gas transfer out of the NC onto the pre-cooled trap T1 in the following 3 min cryogenic pumping step. Afterwards, with the cryopump still active (i.e. T1 still cooled with LN), the NC and T1 are filled with He ($80\,mL\,min^{-1}$) to 1100 mbar, which is slightly above the pressure in section B ($\sim 3$ min). This prevents backflushing from section B to A when they are connected by switching the 3–WV. At this point, the air sample is released by heating T1 to the set temperature of 150 °C and transferred to the pre-cooled trap T2 by the carrier gas ($80\,mL\,min^{-1}$). This step takes another 3 min. The 3–WV is then closed, again separating section A and B. From here on, the sample is in a reduced carrier gas flow environment, and further sample treatment is handled by the automated part of the system as described in Sect. 3.1. Meanwhile section A can be prepared for the next sample. Therefore, the outlet valve of the NC is closed, the $N_2$ flush flow opened and the next ice cube loaded. If the next sample in the sequence (Table 3) is to be measured with the ice remaining in the NC, evacuation of the extraction unit and the vacuum lines is sufficient to prepare for the next run.

For the measurement of natural ice samples, the procedure is as described above but all steps related to the air standard addition can be skipped. Chromatograms of the TCD, PDD and IRMS for a typical ice sample measurement are shown in Fig. 3. Here, as opposed to measurements of pure $CO_2$-WS and blanks (Figs. S1 and S2, respectively), the peak from sample air shows up as a distinct TCD signal, and signals of $H_2O$ from ice sample water vapour and remnants of drilling fluid contamination are detected by the PDD in addition.

Including section A of the system does not add much to the total measurement time given in Sect. 3.1 because most of the additional steps required can already be executed while the current measurement is running in the automated section B. Typically, the analysis takes around 30 min (run to run). However, it increases for runs requiring loading of a new ice sample (opening of the NC) and as a consequence the described evacuation and flushing steps ($\sim 50$ min, e.g. runs 6, 11, 14 and 18 in Table 3).

## 4 Results and discussion

### 4.1 Evaluation and calibration

System-specific analytical bias for $CO_2$ concentration and $CO_2$ stable isotope measurements can result from fractionation in the analytical system related to adsorption and desorption processes, specifically in the extraction unit (Zumbrunn et al., 1982), non-quantitative trapping and releasing of gas and from GC separation. For stable isotope measurements, further bias arises from IRMS injection and source effects (Elsig and Leuenberger, 2010). The net effect of these processes was assessed and monitored on a regular basis to account for system drifts. Such drifts may occur when boundary conditions (e.g. room temperature) change and can appear within a measurement day, on a day to day basis and on longer timescales, here being either related to changes in the set-up (e.g. replacements of parts, change of carrier gas tanks or standards, adjustments in carrier gas flows) or small changes in the procedure. Following the identical treatment principle (Werner and Brand, 2001), we characterized all sections of our system for systematic effects using the various standards available (Table 2), ultimately allowing a reliable correction of the raw data. Runs of QCS to assess long-term stability of our final measurement results were carried out on a daily basis (results in Sect. 4.2.1).

#### 4.1.1 $CO_2$

$CO_2$ mixing ratios can, in principle, be derived from the ratio between the IRMS $CO_2$ peak area (values given in the following always denote the mean for the three sample peaks) and the major air components detected as TCD peak area (Fig. 3). The TCD air peak signal was observed to be nonlinearly related to the amount of air with significant variability. This can be seen in the relation between the high-precision pressure readings of standard gas (described in Sect. 3.2) and the TCD air peak area investigated for different measurement periods (Fig. 4a). We also found variability in the relation between the IRMS peak area and the $CO_2$ amount; in this case, however, the relationship is linear. Reasons for the observed variability are manifold, e.g. small adjustments in flow or trapping procedures, or small changes in outer conditions such as room temperature (e.g. March and June 2012).

**Calibration**: To avoid nonlinearity in data processing, the TCD signal was converted to pressure using the second-order polynomial functions shown in Fig. 4a. These functions can be determined for any user-defined period of time with

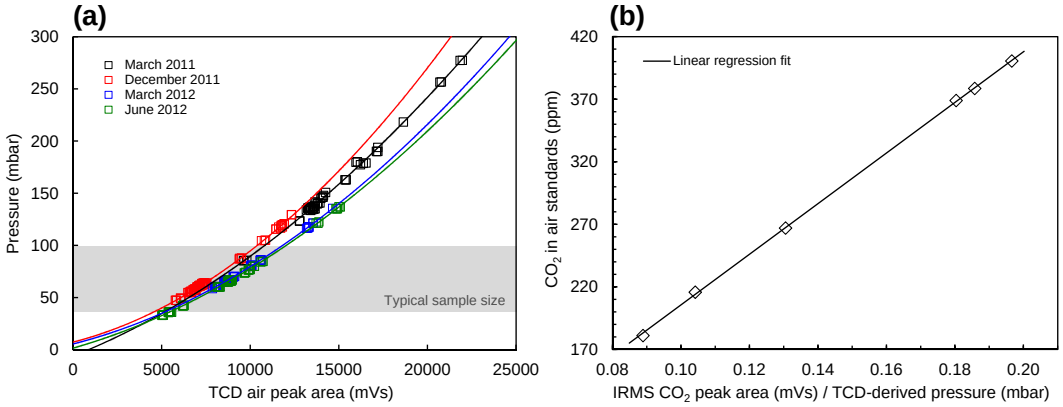


**Figure 4.** $CO_2$ calibration. **(a)** Relationship between sample size and TCD peak area of air for different measurement periods. The lines are second-order polynomial fits through the data. Pressure in the injection volume is proportional to amount. The grey bar indicates the typical sample size range extracted from ice samples. **(b)** Calibration curve; known $CO_2$ mixing ratios of air standards vs. ratio of IRMS peak area for $CO_2$ ($m/z$ 44) and TCD detected air amount transformed to pressure from the relationship shown in **(a)**.

the data obtained from daily performed measurements of air standards. In doing so, the large long-term variations in TCD sensitivity are accounted for and all TCD measurements are adjusted and referred to a common scale (pressure). The $CO_2$ mixing ratios known for the standard gases were then related to the derived ratio between the IRMS $CO_2$ peak area and the computed pressure. By including data of all available standards, the resulting linear calibration curve is well defined over a large concentration range (Fig. 4b). The data shown are based on repeated measurements series over the course of more than 1 year ($n = 4$). Each series was performed on a single day with the entire range of standards being measured at least three times. The ratios calculated for the individual series were matched for CA08054 in order to account for the long-term variation of the IRMS response, resulting in the average transfer function shown.

With the calibration curve covering the entire range of expected measurement results (Fig. 4b), daily calibration could be performed with a subset of standards only, thus significantly reducing the total sequence time. Summarized in Table 3, a typical daily measurement sequence includes the repeated measurement of standard CA08504 (run 8, 10, 13 and 20) to determine and subsequently adjust for (i) potential offset in the calculated ratio compared to the calibration curve and (ii) system drift over the sequence measurement time. It further includes at least one additional standard gas measurement with a different $CO_2$ mixing ratio to adjust for potential variations in the slope of the linear calibration fit (runs 16, 21 and 17 if necessary). If not used in the daily calibration, run 17 is treated as a real sample in the post processing of the raw data, allowing us to assess the long-term consistency and precision of our measurements (QCS; see Sect. 4.2.1). In run 21, CA08504 is occasionally injected in variable amounts to ensure the independence of the final results from the sampled amount of gas.

**Procedural blank**: We find that independently of sample size, gas amount or $CO_2$ concentration, a constant amount of $CO_2$ is produced by the extraction itself. This amount was determined by measurements of BFI samples. To perfectly simulate measurements of natural ice samples according to the identical treatment principle (Werner and Brand, 2001), artificially produced bubble ice with entrapped standard gases would be required. Because this is technically not feasible, instead we added standard gas to a BFI sample loaded in the NC and crushed for the measurement. The $CO_2$ mixing ratios we observed were elevated by $4.6 \pm 2.6$ ppm on average ($n = 5$) compared to the expected value. However, for subsequent measurements with an identical procedure (including movement of the needle pins), but using the previously crushed BFI, the observed elevation was less. This indicates the presence of remnant gases in our BFI which is in agreement with independent results from another study ($\sim 3$ ppm for CIC BFI, Appendix A6 in Rubino et al., 2013). We thus considered the lower offset value of $2.3 \pm 2.0$ ppm (average, $n = 4$) to be representative of the purely system related blank. This is a reduced offset compared to other systems, allowing the analysis of similarly small sample sizes (e.g. 4.9 ppm for the KUP NC; Bereiter et al., 2013) which most likely is a result of the friction-reduced motion and lower operating temperature in our NC design. Anyhow, this $CO_2$ enrichment – expressed in ppm before – is observed in the raw data as an elevated signal in the IRMS $CO_2$ peak area. The size of this extra signal can therefore be directly estimated from procedural blank measurements when using BFI which has been crushed in advance (Fig. S3). As an advantage, propagation of uncertainties associated with data post-processing can then be omitted. Combining the results from both approaches, the IRMS $CO_2$ peak area for the procedural blank was observed to be $0.5 \pm 0.2$ mVs on average ($n = 9$), i.e. elevated by $0.1 \pm 0.1$ mVs compared to the system blank (see

Sect. 4.1.2 – Air amount dependence). In Sect. 4.1.3, the procedural blank correction applied to ice core samples will be discussed in detail.

### 4.1.2 $\delta^{13}$C-$CO_2$ and $\delta^{18}$O-$CO_2$

The individual sections of the set-up were characterized for systematic effects on $\delta^{13}$C and $\delta^{18}$O results. Calibrations, control of system stability and blanks, as well as QCS measurements to assure the long-term quality of our analysis (Sect. 4.2.1), were all performed on a daily basis (Table 3).

**IRMS nonlinearity**: We characterized the IRMS source effects – in the following referred to as IRMS nonlinearity – by measurements of reference gas ($CO_2$-WS) injected via the GP interface reference open split (Fig. 2). To reach stable source conditions, six injections were made prior to acquisition similar to the approach described in Elsig and Leuenberger (2010). Then, the injection amount was increased step-wise, reflected in rising amplitudes of the rectangular peaks. The signal amplitude thereby ranged between 400 and 8400 mV ($m/z$ 44), with the reference peak always set to around 4000 mV (gain: $R = 10^8\Omega$). This experiment was replicated on three different days distributed over a time period of 1 year. The resulting total number of acquisitions was 177. In Fig. 5a, the IRMS nonlinearity effect for $\delta^{13}$C is shown, measured as the deviation from the reference ($\sim$ 4000 mV). The same procedure was applied to investigate the $\delta^{18}$O nonlinearity (Fig. S3).

**PreCon–GC linearity**: A potential and possibly size-dependent effect on the stable isotope values of the sampled gas when passing the various traps and GC columns in the automated set-up section B (Fig. 2) was investigated. Therefore, various amounts of the $CO_2$-WS were injected onto trap T2 via the injV (Fig. 2) as described in Sect. 3.1. The relationship found will be denoted as PreCon–GC linearity in the following. In addition, the blank for this section was determined when injection of $CO_2$ was omitted, but otherwise the exact same procedure was followed (Sect. 3.1). To allow determination of this PreCon–GC-related effect independently from any other system-induced contribution, the obtained raw data were first corrected for the IRMS nonlinearity by applying the third-order polynomial fit shown in Fig. 5a. Subsequently, a blank correction using the values determined here was applied. Therefore, the following equation which closely approximates the isotopic composition in a pool ($\delta_\Sigma$) of isotopically different members ($m_i$ with corresponding $\delta_i$) was used:

$$\delta_\Sigma = \frac{\Sigma\, m_\mathrm{i}\delta_\mathrm{i}}{\Sigma\, m_\mathrm{i}}. \quad (2)$$

Equation (2) shows that the bigger the $CO_2$ blank-to-sample ratio and the difference between blank and sample isotopic composition, the bigger the blank correction will be. In other words, even when the blank is constant both in size and isotopic composition, the blank correction should vary depending on the $CO_2$ mixing ratio, the isotopic composition and the gas amount of the sample analysed. Therefore, it is essential to carefully separate effects on the observed isotopic signal related to the blank from all other system-induced effects. If ignored, any determined relationships will only be valid for samples of identical size, $CO_2$ mixing ratio and isotopic composition as the standard gas used for its determination. As a result, a scale compression bias may arise if applied to all samples anyway. Corrected for the blank initially, the PreCon–GC linearity determined here is valid for the correction of any sample (Fig. 5b). The corresponding relationship for $\delta^{18}$O can be found in the Supplement (Fig. S3). It needs to be noted that the isotopic values of the blanks are affected equally by system-induced fractionation effects as those of any other sample and similar correction needs to be applied. Therefore, the values used for the blank correction and the final relationship shown in Fig. 5b (and

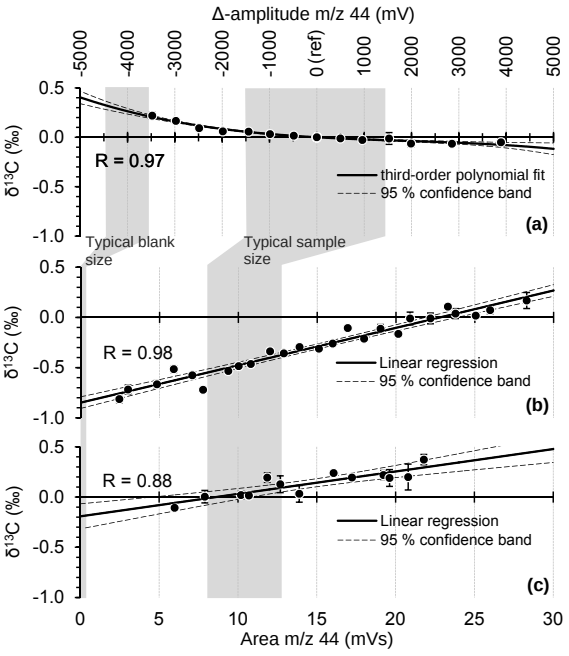


**Figure 5.** Fractionation effects for $\delta^{13}$C: **(a)** IRMS nonlinearity; $\delta^{13}$C dependence on peak amplitude (top $x$ axis), $\Delta-$amplitude is the deviation in intensity ($m/z$ 44) from the reference peak (ref, $\delta^{13}$C and $\Delta-$amplitude $= 0$). The data are obtained from a total of 177 measurements and mean values with the $1\sigma$ standard deviation are shown. **(b)** PreCon–GC linearity (bottom $x$ axis); $CO_2$ sample size dependence for pure $CO_2$ working standard directly injected to section B. The data are obtained from a total of 318 measurements corrected for IRMS nonlinearity and blank; mean values with the $1\sigma$ standard deviation are shown. **(c)** Air amount dependence (bottom $x$ axis); air sample size dependence for air standards/samples injected to section A. The data are obtained from a total of 46 measurements corrected for IRMS nonlinearity, PreCon–GC linearity and system blank. Mean values with the $1\sigma$ standard deviation are shown. The grey bars indicate the typical procedural blank and sample size range of air extracted from ice samples, respectively.

Fig. S3 for $\delta^{18}O$) were derived iteratively until changes in the converging values were well below the IRMS precision ($n = 5$). The final mean values for blanks ($n = 99$) which were reproducible for the acquired 2-year time period were $0.09 \pm 0.02$ mVs, $-24.2 \pm 1.9$ ‰ and $-41 \pm 5$ ‰ for $CO_2$ IRMS peak area, $\delta^{13}C$ and $\delta^{18}O$, respectively. This demonstrates that the blank isotopic values are strongly depleted compared to atmospheric values. This is consistent with the assumption that the blank is related to tiny amounts of $CO_2$ constantly being adsorbed and desorbed from inner surfaces, trapping materials and GC columns, thereby undergoing heavy isotopic fractionation. To test if the measured values are reliable although measured on extremely small sample amounts, comparable amounts of $CO_2$-WS were directly injected via the sample open split, resulting in a similar peak shape ($n = 5$, IRMS peak area between 0.14 and 1.17 mVs). After correction for the IRMS nonlinearity effect, we obtained average values of $-6.5 \pm 0.6$ ‰ and $-11.7 \pm 1.6$ ‰ for $\delta^{13}C$ and $\delta^{18}O$, respectively. These numbers are not significantly different from the expected values for the $CO_2$-WS ($-6.004 \pm 0.008$ ‰ and $-10.80 \pm 0.13$ ‰), which demonstrates the reliability of measurements for such small sample amounts and adds confidence to the determined blank values.

**Air amount dependence**: To investigate the characteristics of the system section A, variable amounts of the CA08054 air standard were analysed over ice. Changing the gas matrix from pure $CO_2$ to trace amounts in air may cause alteration in the previously defined PreCon-GC linearity. This potential effect cannot be distinguished in this experiment and may contribute to the observations in the following being denoted as the "air amount dependence". In repeated series ($n = 10$), distributed over a time period of more than 1 year, 46 such measurements were made. In addition, 42 blanks (omitting sample injection but exactly following the procedure otherwise) were measured. Following the approach for determination of the PreCon–GC linearity, the blank contribution was separated from the effect investigated here. Identical to samples, blanks were corrected for IRMS nonlinearity, PreCon–GC linearity and the air amount dependence discussed here again in an iterative way. The blank value obtained, now representative of the entire set-up and accordingly denoted as "system blank", was $0.4 \pm 0.1$ mVs, $-27.6 \pm 1.2$ ‰ and $-30 \pm 3$ ‰ for $CO_2$ peak area, $\delta^{13}C$ and $\delta^{18}O$, respectively. Because of the additional trap (T1) and large additional surface area from extra lines and the NC chamber, the bigger size of the system blank compared to the blank observed for the PreCon–GC section alone is expected. However, the obtained values for their isotopic composition are comparable. This indicates the responsible fractionation effects, likely related to adsorption and desorption processes, to be similar in the different sections of the set-up. Because the built-in parts are alike in surface and trapping material, this is not unexpected. The final relationship for the air amount dependence is presented in Fig. 5c. As described, it was obtained after correction for IRMS nonlinearity, PreCon–GC linearity and blank contribution (for $\delta^{18}O$ see Fig. S3).

**Procedural blank**: The procedural blank determined in Sect. 4.1.1 was also analysed for its isotopic composition. The isotope ratios resulted in values of $-26.6 \pm 0.8$ ‰ for $\delta^{13}C$ and $-29 \pm 3$ ‰ for $\delta^{18}O$ ($n = 5$) when using BFI which has been crushed in advance to avoid artefacts from entrapped remnant gas. Because the available amount of gas for such measurements is very small ($0.5 \pm 0.2$ mVs), a second indirect approach based on larger sample sizes was applied. Thereby, the same standard was analysed twice, simulating the crushing procedure with BFI in the second measurement. Nine such sets were measured and in four of them, the BFI used has already been crushed in advance. In addition to the already known amount of the $CO_2$ procedural blank contribution, for each set, the isotopic composition expected for the standard and the amount of the $CO_2$-total with its isotopic composition is defined by the first and second measurement, respectively. With these numbers as input values, the isotopic composition of the procedural blank could then be estimated using a reversed form of Eq. (2). The values derived in this way for the procedural blank were $-24 \pm 3$ ‰ and -28 ± 4 for $\delta^{13}C$ and $\delta^{18}O$, respectively ($n = 9$). The bias due to the small amounts of remnant gas in the BFI can be calculated (Eq. 2) to be of the order of 0.2 ‰ and can thus be neglected considering the uncertainty of this approach. In any case, these results are in close agreement with those obtained by the direct measurement of the procedural blank and further verification of their strongly depleted isotopic composition. In Sect. 4.1.3, the procedural blank correction ultimately applied to ice samples will be discussed.

**Calibration**: All raw data were post-processed, correcting for the characterized effects in the given order: (1) IRMS nonlinearity, (2) PreCon–GC linearity, (3) air amount dependence and (4) blank contribution. The repeated measurements of air standards differing in their $CO_2$ mixing ratio and isotopic composition were then used for daily calibration to adjust for potential day by day offsets and daily drift (runs 8, 10, 13, 16, 20, 21 and 17 in some cases). If not used for calibration, run 17 was treated as a QCS (see Sect. 4.2.1). For run 21, CA08504 is occasionally injected in variable amounts to ensure the independence of final results from the sampled gas amounts. Results and achieved precision for the measurements of ice samples will be discussed in Sect. 4.2.2.

### 4.1.3 Procedural blank correction

For any analytical application, a thorough assessment and quantification of the blank is crucial. Whereas the system blank usually is representative for the analysis of standards ultimately used for calibration of the results, the procedural blank – here related to the measurement of ice core samples – can include extra contribution from sample treatment (e.g. preparation and crushing).

**$CO_2$**: to account (i.e. correct) for the extra contribution of the procedural blank compared to the system blank, the common approach described in the literature for measurements of $CO_2$ and its stable isotopes in ice core samples is to ultimately subtract a constant offset (e.g. Elsig et al., 2009; Schmitt et al., 2011; Rubino et al., 2013). Here, for $CO_2$ results this offset would correspond to the $2.3 \pm 2.0$ ppm determined in Sect. 4.1.1. However, such an approach requires the assumption that the extra $CO_2$ contribution of the procedural blank is variable in terms of amount (i.e. moles) in such a way, that the offset results in a constant blank-to-sample ratio regardless of $CO_2$ concentration and amount of sample gas extracted from the ice. Only then will a constant offset in terms of ppm (parts per million by volume) result. As this is highly unlikely, a compressed scale for data covering a large range of $CO_2$ mixing ratios has to be expected. As an example, this would be the case for records of glacial to interglacial atmospheric conditions ranging from around 180 ppm to the current atmospheric level of around 400 ppm. Whereas for measurements with large sample sizes, i.e. low blank-to-sample ratios, such a bias might be negligible, a different, more accurate correction of the procedural blank should be applied particularly if using small samples. In agreement with our observations of the blank, we here assumed the extra $CO_2$ contribution to be constant in terms of the absolute amount (moles not mole fraction/i.e. ppm). Accordingly, for each ice sample we subtracted the signal determined for this additional $CO_2$ contribution (Sect. 4.1.1) from the measured IRMS $CO_2$ peak area prior to conversion of results into ppm. For the small sample sizes analysed here, the improvement of this approach is directly reflected in a reduced standard deviation for results from sets of replicate ice measurements (same site and sampling depth, variable in the sampled gas amount; see Sect. 4.2.2 for sample details). For these samples, the applied correction varied between 1.9 and 3.3 in terms of ppm (2.4 ppm on average, $n = 18$).

**$\delta^{13}C$ and $\delta^{18}O$**: for the procedural blank correction of isotopic values, the common approach of subtracting a constant offset is even more critical. As discussed in Sect. 4.1.2 (PreCon–GC linearity), even for blanks constant in $CO_2$ contribution and isotopic composition, the magnitude of the procedural blank correction should be dependent on the sample size as well as the sample $CO_2$ mixing ratio and isotopic composition. Obviously, the bigger the $CO_2$ blank-to-sample ratios and the difference between blank and sample isotopic composition, the bigger the correction will be. Considering the observed strongly depleted isotopic composition of the blank $CO_2$ (Sect. 4.1.2), the variation of the correction might be significant even for samples of larger size. For sample sizes 10 times bigger than the ones analysed in this study (i.e. $\sim 100$ g ice), the scale compression bias resulting from the application of the conventional approach was calculated for an ice core record covering the Holocene (approximated range: 180 to 370 ppm in $CO_2$ and $-6.3$ to $-6.6$ ‰ in $\delta^{13}C$). For the $\delta^{13}C$ of the procedural blank, the determined low value of $-26.6$ ‰ was used (Sect. 4.1.2). The procedural blank for the conventional correction of $CO_2$ and $\delta^{13}C$ was assumed to be 1 ppm and 0.1 ‰, respectively. These are typical literature values and small compared to the numbers determined in this study. Employing Eq. (2) for calculation, a potential additional effect arising from variations in the ice sample size used to obtain the record is not considered. Nevertheless, the expected scale compression bias is calculated to be around 0.06 ‰ for the commonly applied procedural blank correction. This demonstrates that even for larger sample sizes, this bias can be significant, considering the recent improvements in analytical precision. Obviously, it is of particular relevance for higher blank-to-sample ratios (e.g. small sample sizes). Here we thus applied a new, more accurate approach for the procedural blank correction. It is similar in principle to the description given in Sect. 4.1.2 for air standards and is based on Eq. (2). We used $0.5 \pm 0.2$ mVs, $-26.6 \pm -0.8$ ‰ and $-29 \pm 3$ ‰ for procedural blank size, $\delta^{13}C$ and $\delta^{18}O$, respectively (Sect. 4.1.2). The results and precision for measurements of natural ice samples will be discussed in Sect. 4.2.2.

## 4.2 System performance

### 4.2.1 Analytical precision for the measurement of air samples

The precision and long-term consistency of our measurements were assessed by repeated QCS measurements of the two air standards AL-1 and AL-2 injected over natural and artificial (BFI) ice both before and after crushing. These two standards are different in their $CO_2$ mixing ratios and isotopic compositions (Table 2) and were injected in variable amounts of gas. QCS measurements were treated similarly to real ice samples, both in the applied measurement procedure (except for the crushing step) and the post-processing of the acquired raw data. In Fig. 6, the resulting time series for $CO_2$, $\delta^{13}C$ and $\delta^{18}O$ covering a 2-year period are shown. To derive a completely independent assessment, QCS measurements used in the daily calibration routine were excluded for this analysis. For the time frame covered, no trend can be observed for either of the parameters analysed in the two standards. The determined and assigned values agree well within the uncertainties. However, a small systematic shift of unknown origin observed for $\delta^{18}O$ of AL-2 cannot be excluded. From the combined dataset of AL-1 and AL-2 shown in Fig. 6, our analytical precision for the measurement of air samples over ice was determined with 1.9 ppm, 0.09 and 0.16 ‰ for $CO_2$, $\delta^{13}C$ and $\delta^{18}O$, respectively (standard deviations around the respective mean).

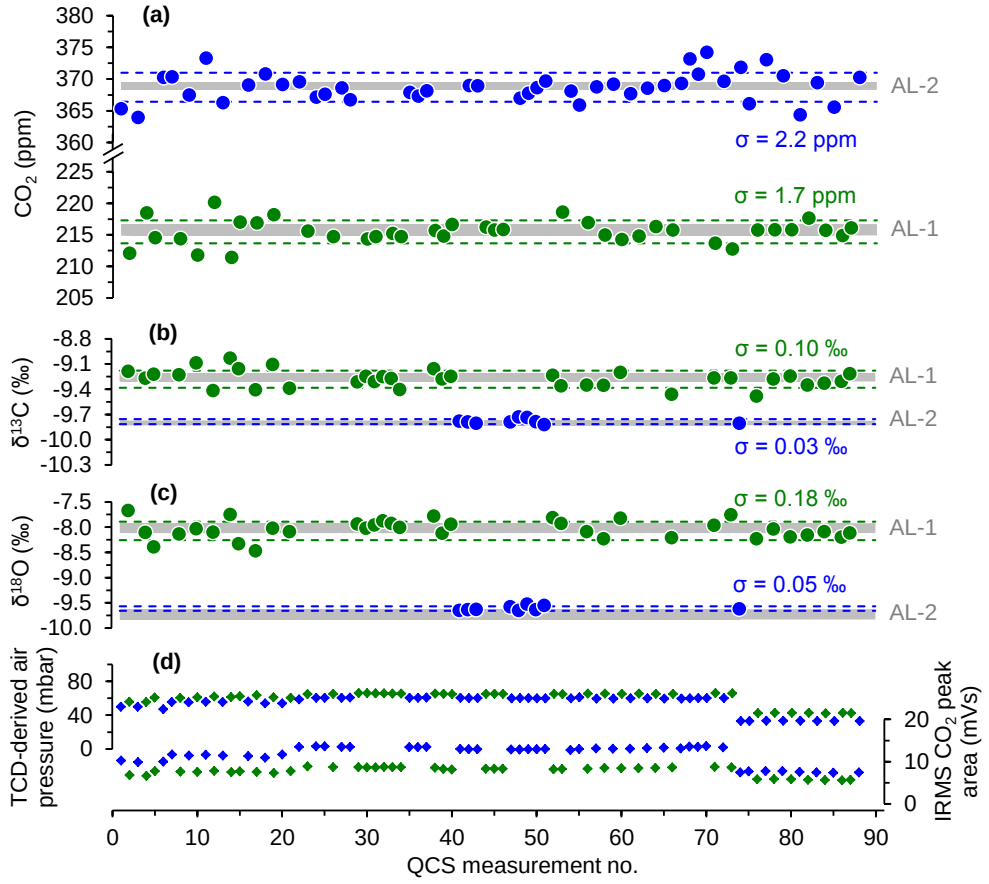


**Figure 6.** Repeated quality control sample (QCS) measurements of air standards AL-1 (in green) and AL-2 (in blue) over ice, covering a time period of 2 years. The grey bands indicate the assigned value of the standard with uncertainty as given in Table 2. Dashed lines indicate the $1\sigma$ standard deviation of the data points (see numerical values). **(a)** $CO_2$ mixing ratios (ppm). **(b)** $\delta^{13}$C-$CO_2$ (‰ VPDB). **(c)** $\delta^{18}$O-$CO_2$ (‰ VPDB-$CO_2$). **(d)** Injected amount of air (top, left axis) and related amount of $CO_2$ (bottom, right axis). Fewer results are shown for the stable isotopes because standards used in the daily calibration routine (i.e. not post-processed similar to real samples) were excluded from this analysis.

#### 4.2.2 Natural ice samples – laboratory comparison and reproducibility

From measurements of ice samples from various sites and depths (8–13 g), the extraction efficiency of our NC was determined by the amount of air liberated, divided by the expected air total in the sample. Typically the efficiency is around 70–80 % for bubbly ice and around 60 % for clathrate ice (with the gas release time after crushing extended by 4 min). This is in the similar range as reported for other NC designs (Ahn et al., 2009; Lüthi, 2009; see Table 1).

To demonstrate the system performance and reproducibility, we analysed six ice samples of the recent past (1851–1969 AD) from Law Dome, Antarctica (DE08, 66°43′ S, 113°12′ E). This was done in a comparison study with CSIRO. The range of sample ages allowed for a comparison across a relatively wide range of $CO_2$ and $\delta^{13}$C values. These samples were also part of an independent study published earlier (Rubino et al., 2013). Note that DE08 was dry-drilled and therefore the difference in the measurement systems that addresses drilling fluid contamination (i.e. separation by GC in the CIC system) is not tested. We measured replicates ($n = 2$ to 4) on the egg-shaped pieces remaining after the samples have been processed at CSIRO using their cheese grater dry extraction system. To allow a realistic assessment of measurement reproducibility, the replicates were measured on different days. The pooled standard deviation, used as a measure to estimate the overall analytical precision of our system for single measurements, was 2.0 ppm and 0.11 ‰ for $CO_2$ and $\delta^{13}$C, respectively ($n = 18$). Compared with the results from CSIRO, good agreement within the assigned $1\sigma$ uncertainties was found for both $CO_2$ and $\delta^{13}$C (Fig. 7). While the agreement between $\delta^{13}$C results is high (average CIC – CSIRO = 0.02 ‰), a small systematic offset of +1.8 ppm seems to exist for $CO_2$. An obvious explanation for this offset would be discrepancies in calibration between the two laboratories relying on independent standards.

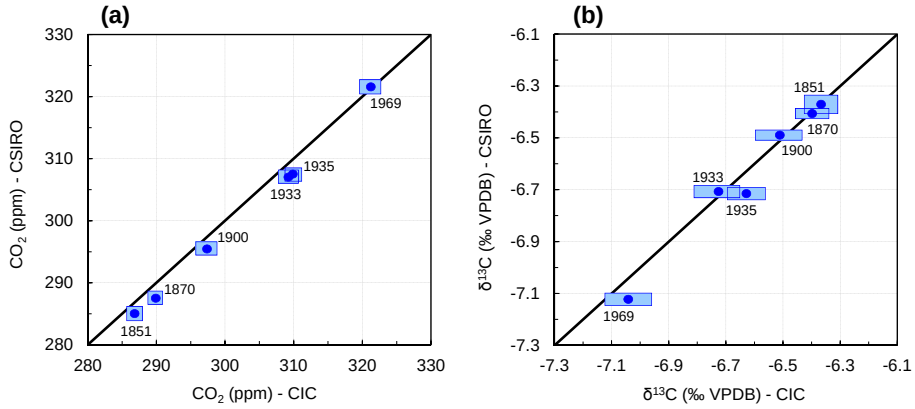


**Figure 7.** Laboratory intercomparison measurements between CIC and CSIRO of Law Dome ice core samples covering the recent past (1851–1969 AD). $CO_2$ mixing ratios **(a)** and $\delta^{13}$C-$CO_2$ values **(b)** measured at CIC ($x$ axis) and CSIRO ($y$ axis; Rubino et al., 2013) are shown. Blue boxes indicate $1\sigma$ uncertainties defined for each laboratory by the respective side length.

This is however not supported by the good agreement for the comparison of air tank measurements with different $CO_2$ mixing ratios ($-0.3$ ppm on average, $n = 3$). Alternatively, the observed offset could be a real signal, explained by the occlusion of ambient air in micro-cracks resulting from the fierce mechanical treatment in the CSIRO grater and the elevated temperatures recorded during ice transport preceding the CIC measurements (around $-5$°C). For the same reason, the deviation in results of replicate measurements may partly be influenced by the ice itself, i.e. causing analytically independent variability. We therefore consider the pooled standard deviation calculated for the Law Dome samples to be a rather conservative estimate of our overall analytical uncertainty for single ice sample measurements. The estimate is however in line with the uncertainty determined for the QCS measurements (Sect. 4.2.1) with a slightly larger uncertainty to be expected for the measurements of ice considering size and uncertainty of the procedural blank compared to the system blank correction. In any case, due to the benefit of the small sample size required by our method, execution of replicate measurements is feasible even though the availability of samples from ice cores is limited. The achievable overall method precision for a measurement based on $n$ ice sample replicates can thus potentially be increased by $(n)^{-0.5}$ compared to the uncertainty defined for a single measurement. For $\delta^{18}$O, the pooled standard deviation is 0.32 ‰ ($n = 18$) and the offset between the two laboratories was 0.5 ‰ on average (Fig. S4). These values should be viewed cautiously. Oxygen exchanges between $CO_2$ and $H_2O$ from the surrounding ice matrix (Friedli et al., 1984; Siegenthaler et al., 1988; Assonov et al., 2005; Bauska et al., 2014). Due to its strong seasonal cycle, $\delta^{18}$O-$H_2O$ can be expected to vary between adjacent samples even for the high CIC sampling resolution. Because of the oxygen exchange, $\delta^{18}$O-$CO_2$ does pick up the seasonal $\delta^{18}$O cycle present in the ice (see Fig. S5 and Sect. 4.3) although no seasonality is initially retained in the gas because of signal smoothing in the firn. This will lead to analytically independent variability in replicates of $\delta^{18}$O-$CO_2$ measurements. Accordingly, the uncertainty estimated from the observed variation between the DE08 replicates is expected to be too high. The sample history discussed before (i.e. mechanical pre-treatment and transport) may be another contributing factor. Considering the differences in sample size and resolution used at CSIRO and CIC, the oxygen exchange may also (partly) explain the deviation of inter-laboratory $\delta^{18}$O-$CO_2$ results. For a summary of the main analytical system characteristics see Table 1.

### 4.3 Outlier detection based on $\delta^{18}$O-$CO_2$ and $\delta^{18}$O-$H_2O$

$CO_2$ exchange with the terrestrial biosphere dominates the signal of the $^{18}O/^{16}O$ ratio in atmospheric $CO_2$. Therefore, atmospheric $^{18}$O-$CO_2$ is a valuable proxy to constrain changes in terrestrial primary production and the hydrological cycle (e.g. Farquhar et al., 1993). However, $^{18}$O-$CO_2$ measured in ice cores is affected by the exchange of oxygen with the ice matrix. This has been demonstrated by measurements of samples from different sites and time periods (Friedli et al., 1984; Siegenthaler et al., 1988; Bauska et al., 2014) as well as in firn gas (Assonov et al., 2005).

Here, we present a new approach for analytical quality control, based on $\delta^{18}$O-$CO_2$ measurements. It allows reliable and consistent rejection of results from samples which were affected by analytical problems or suffered contamination during e.g. storage or gas extraction. Different sections from GRIP and NGRIP with gas ages of 260 to 1770 years (bags GRIP-250 and GRIP-360, NGRIP-213 and NGRIP-696) and 25 000 years (bags GRIP-3628 and GRIP-3636) were analysed in high spatial and temporal resolution of 2.5 cm and < 1 year (ice age scale), respectively. Parallel samples (same depth) were measured for $\delta^{18}$O-$H_2O$ in similar resolution if no data existed already. Similar to the previ-

ous studies, high correlation between $\delta^{18}$O-$CO_2$ and $\delta^{18}$O-$H_2O$ was observed (Fig. S5). With this dataset, the expected $\delta^{18}$O-$CO_2$ value in the following denoted as $\delta^{18}$O-$(CO_2\text{-ice})_{eq}$ could be calculated for each sample from its corresponding $\delta^{18}$O-$H_2O$ value, considering oxygen exchange in thermodynamic equilibrium between gaseous $CO_2$ and the surrounding ice matrix. We thereby followed the approach by Siegenthaler et al. (1988), combining the thermodynamic equilibrium oxygen isotope fractionation factors $\alpha$ for ($CO_2$- $H_2O_{(l)}$), ($H_2O_{(l)}$-$H_2O_{(g)}$) and ($H_2O_{(g)}$-$H_2O_{(s)}$) given therein. It should be noted that this approach might not be valid particularly for ice from very cold sites because it assumes that those values for $\alpha$ which for obvious reasons could be determined experimentally only for temperatures above the freezing point of water can be linearly extrapolated to lower temperatures (< 273.15 K). Using the same approach for a site with annual mean temperatures of −26 °C (Berkner, Antarctica), the time to reach 50 % of the thermodynamic equilibrium ($T^1/_2$) was empirically determined to be around 23 years (Assonov et al., 2005). The site temperatures for GRIP and NGRIP are comparable (around −30 °C). It can therefore be assumed that even the youngest samples analysed in this study have reached complete equilibrium in the glacier. However, the GRIP and NGRIP ice cores were drilled in 1992 and from 1996 to 2004, respectively. From the time the cores have been recovered, a new thermodynamic equilibrium now driven by the storage temperature needs to be considered. For $T^1/_2$ and storage durations of ∼ 15 and 20 years until the time of measurement, the degree of the new equilibrium reached is only 30 and 45 % for NGRIP and GRIP samples, respectively. To take the temperature exposure history of the ice into account, the equilibrium temperature was defined as the weighted mean of borehole temperature at sampling site depth (around −30 °C; Johnsen et al., 1995; Dahl-Jensen et al., 2003) and freezer temperature (−23 °C). Accordingly, the freezer temperature was weighted with 0.30 for NGRIP and 0.45 for GRIP. The uncertainty of the mean equilibrium temperature (−28 °C) was estimated by propagating a 10 % uncertainty for the degree of the equilibrium and an error of 2 °C each for borehole and storage temperatures. In Fig. 8, the correlation between the observed and the theoretical $\delta^{18}$O-$CO_2$ is shown. Overall, the agreement between measured and theoretical values is high ($R = 0.90$) with a small offset of 0.05 ‰ on average. This is a strong indication for the occurrence of oxygen exchange between $CO_2$ and $H_2O$ within the ice archive and in agreement with previous observations (e.g. Siegenthaler et al., 1988). The 1$\sigma$ standard deviation around the theoretical equilibrium line was 0.8 ‰, exceeding the estimated analytical precision by more than a factor of 2. Based on that, we defined an outlier identification criterion for samples where $\delta^{18}$O-$CO_2$ differed by more than 1.6 ‰ (2$\sigma$) from the theoretical value (Figs. 8 and S5). For these samples, the $CO_2$ and $\delta^{13}$C measured values were rejected from the analyses. In all cases the rejected samples showed suspicious values in both

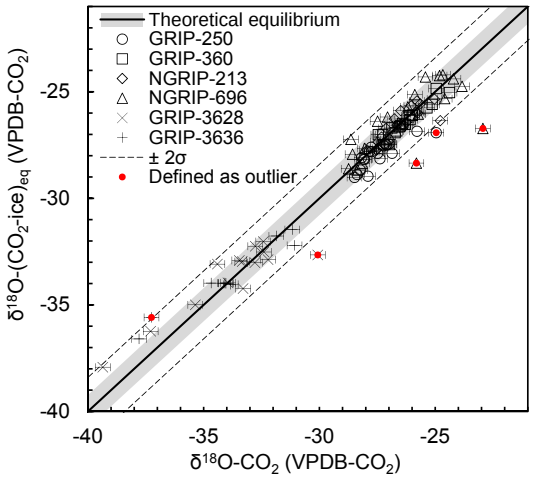


**Figure 8.** $\delta^{18}$O-$CO_2$ used as a quality control tool for ice core measurements. The correlation between measured ($x$ axis) and expected ($y$ axis) $\delta^{18}$O-$CO_2$ is shown for samples from GRIP and NGRIP measured in high spatial and temporal resolution for sections with gas ages of 260 to 1770 years and 25 000 years. The expected $\delta^{18}$O-$CO_2$ was derived considering thermodynamic equilibrium of gaseous $CO_2$ with the surrounding ice matrix and is accordingly denoted as $\delta^{18}$O-$(CO_2\text{-ice})_{eq}$. The calculated theoretical equilibrium (black line) is shown with an uncertainty band (grey), accounting for the error associated with equilibrium temperature estimates. The dashed line indicates the 2$\sigma$ standard deviation around the theoretical value considering all data points shown. For samples outside this range (red dots) $CO_2$ and $\delta^{13}$C-$CO_2$ results were rejected.

$CO_2$ and $\delta^{13}$C, but because no obvious reason such as issues with the analytical system was noticed (e.g. bad vacuum, trap temperatures being out of range), they could not have been consistently removed otherwise. Unnoticed micro-cracks in the ice might be the most likely explanation for these outliers.

## 5 Conclusions and outlook

This study describes a new analytical set-up for simultaneous measurements of atmospheric $CO_2$ mixing ratios and atmospheric $\delta^{13}$C and $\delta^{18}$O-$CO_2$ in air extracted from ice core samples. The centrepiece of the system is a newly designed needle cracker for mechanical dry extraction, operated at an extra low temperature of −45 °C. With this set-up the throughput of three to four samples per day and the small amount of ice required (8–13 g) enables a high resolution.

We discussed analytical procedures, systematic linearity testing for the various system parts, daily calibration as well as data processing. Determined from repeated long-term quality control measurement of air samples over ice (natural and BFI), high analytical precision was achieved, being 1.9 ppm for $CO_2$ and 0.09 ‰ for $\delta^{13}$C. Law Dome ice core

samples were analysed in a laboratory intercomparison study with CSIRO, and good agreement between the two laboratories was found for $CO_2$ and $\delta^{13}C$. Replicate analysis of these samples was performed on different days and resulted in a pooled standard deviation of 2.0 ppm for $CO_2$ and 0.11 ‰ for $\delta^{13}C$. Due to the properties of the ice analysed, these numbers may be rather conservative estimates of the achieved overall analytical system precision for single measurements. The potential method precision is higher for results derived from replicate measurements, feasible because of the small sample requirement of the system. In conclusion, our system is well calibrated and the precision comparable to other systems using samples of similar small sizes.

Further, a new approach was proposed for the correction of the procedural blank, leading to more accurate results particularly for the measurements of small samples. Analysis of $\delta^{18}O$-$CO_2$ and $\delta^{18}O$-$H_2O$ confirmed the previously observed exchange of oxygen between $CO_2$ and the surrounding ice matrix occurring within the archive. Based on this, we introduced a new approach for analytical outlier detection which allows reliable and consistent rejection of results from samples affected by analytical problems or some sort of contamination.

Methodological improvement could be achieved through higher extraction efficiency, further reduction in system blank size by optimizing dimensions of connecting lines and traps and by an increased system automation (gas manifold, vacuum lines).

**The Supplement related to this article is available online at doi:10.5194/amt-9-3687-2016-supplement.**

*Acknowledgements.* This work was partly funded by the Centre for Ice and Climate through the Danish National Research Foundation (DNRF) and the European Union's Seventh Framework programme (FP7/2007–2013) under grant agreement no. 243908, "Past4Future. Climate change – Learning from the past climate". CSIRO's contribution was supported in part by the Australian Climate Change Science Program, an Australian government initiative. Thanks are due to the teams involved in recovering and analysis of GRIP, NGRIP and Law Dome sample. We highly appreciate the excellent work done at the Niels Bohr Institute workshop at Copenhagen University. Special thanks is expressed to E. Kaimer for help with all the technical aspects of the NC design and to C. Mortensen, A. Boisen, J. Jørgensen, M. Christensen, D. Westphal Wistisen and S. Sheldon for final manufacturing of the unit, the production of various system components and technical support. Credit goes to T. Popp and B. M. Vinther from the CIC stable isotope laboratory for $\delta^{18}O$-$H_2O$ data and measurements and to C. Allison, S. Coram and R. Langenfelds for their contribution related to CSIRO gas measurements. Thanks are also due to P. Sperlich, C. Buizert, C. Stowasser, M. Guillevic and C. Reutenauer for discussions, input and all the hours spent in the laboratory. Finally, many thanks are expressed to the entire CIC team for scientific exchange and the excellent working environment, particularly to Dorthe Dahl-Jensen who made this all happen.

Edited by: R. Koppmann
Reviewed by: two anonymous referees

## References

Ahn, J. H., Brook, E. J., and Howell, K.: A high-precision method for measurement of paleoatmospheric $CO_2$ in small polar ice samples, J. Glaciol., 55, 499–506, 2009.

Anklin, M., Barnola, J.-M., Schwander, J., Stauffer, B., and Raynaud, B.: Processes affecting the $CO_2$ concentrations measured in Greenland ice, Tellus, 47 B, 461–470, 1995.

Assonov, S. S., Brenninkmeijer, C. A. M., and Jöckel, P.: The $^{18}O$ isotope exchange rate between firn air $CO_2$ and the firn matrix at three Antarctic sites, J. Geophys. Res.-Atmos., 110, D18310, doi:10.1029/2005JD005769, 2005.

Barnola, J.-M., Anklin, M., Porcheron, J., Raynaud, D., Schwander, J., and Stauffer, B.: $CO_2$ evolution during the last millenium as recorded by Antarctic and Greenland ice, Tellus, 47B, 264–272, 1995.

Bauska, T. K., Brook, E. J., Mix, A. C., and Ross, A.: High-precision dual-inlet IRMS measurements of the stable isotopes of $CO_2$ and the $N_2O/CO_2$ ratio from polar ice core samples, Atmos. Meas. Tech., 7, 3825–3837, doi:10.5194/amt-7-3825-2014, 2014.

Bauska, T. K., Joos, F., Mix, A. C., Roth, R., Ahn, J., and Brook, E. J.: Links between atmospheric carbon dioxide, the land carbon reservoir and climate over the past millennium, Nature Geosci., 8, 383–387, doi:10.1038/ngeo2422, 2015.

Bereiter, B., Stocker, T. F., and Fischer, H.: A centrifugal ice microtome for measurements of atmospheric $CO_2$ on air trapped in polar ice cores, Atmos. Meas. Tech., 6, 251–262, doi:10.5194/amt-6-251-2013, 2013.

Bereiter, B., Fischer, H., Schwander, J., and Stocker, T. F.: Diffusive equilibration of $N_2$, $O_2$ and $CO_2$ mixing ratios in a 1.5-million-years-old ice core, The Cryosphere, 8, 245–256, doi:10.5194/tc-8-245-2014, 2014.

Bereiter, B., Eggleston, S., Schmitt, J., Nehrbass-Ahles, C., Stocker, T. F., Fischer, H., Kipfstuhl, S., and Chappellaz, J.: Revision of the EPICA Dome C $CO_2$ record from 800 to 600 kyr before present, Geophys. Res. Lett., 42, 542–549, doi:10.1002/2014gl061957, 2015.

Berner, W., Oeschger, H., and Stauffer, B.: Information on the $CO_2$ cycle from ice core studies, Radiocarbon, 22, 227–235, 1980.

Dahl-Jensen, D., Gundestrup, N., Gorgineni, S. P., and Miller, H.: Basal melt at NorthGRIP modeled from borehole, ice-core and radio-echo sounder observations, Ann. Glaciol., 37, 207–212, 2003.

Delmas, R. J., Ascencio, J.-M., and Legrand, M.: Polar ice evidence that atmospheric $CO_2$ 20,000 yr BP was 50 % of present, Nature, 284, 155–157, 1980.

Elsig, J., Schmitt, J., Leuenberger, D., Schneider, R., Eyer, M., Leuenberger, M., Joos, F., Fischer, H., and Stocker, T. F.: Stable isotope constraints on Holocene carbon cycle changes from an Antarctic ice core, Nature, 461, 507–510, 2009.

Elsig, J. and Leuenberger, M. C.: $^{13}C$ and $^{18}O$ fractionation effects on open splits and on the ion source in continuous flow isotope ratio mass spectrometry, Rapid Commun. Mass Sp., 24, 1419–1430, doi:10.1002/rcm.4531, 2010.

Etheridge, D. M., Steele, L. P., Langenfields, R. L., Francey, R. J., Barnola, J.-M., and Morgan, V. I.: Natural and anthropogenic changes in atmospheric $CO_2$ over the last 1000 years from air in Antarctic ice and firn, J. Geophys. Res., 101, 4115-4128, 1996.

Farquhar, G. D., Lloyd, J., Taylor, J. A., Flanagan, L. B., Syvertsen, J. P., Hubick, K. T., Wong, S. C., and Ehleringer, J. R.: Vegetation Effects on the Isotope Composition of Oxygen in Atmospheric $CO_2$, Nature, 363, 439–443, doi:10.1038/363439a0, 1993.

Francey, R. J., Allison, C. E., Etheridge, D. M., Trudinger, C. M., Enting, I. G., Leuenberger, M., Langenfelds, R. L., Michel, E., and Steele, L. P.: A 1000-year high precision record of $\delta^{13}C$ in atmospheric $CO_2$, Tellus Ser. B-Chem. Phys. Meteorol., 51B, 2, 170–193, doi:10.1034/j.1600-0889.1999.t01-1-00005.x, 1999.

Friedli, H., Moor, E., Oeschger, H., Siegenthaler, U., and Stauffer, B.: $^{13}C/^{12}C$ ratios in $CO_2$ extracted from Antarctic ice, Geophys. Res. Lett., 11, 1145–1148, doi:10.1029/GL011i011p01145, 1984.

Güllük, T., Slemr, F., and Stauffer, B.: Simultaneous measurements of $CO_2$, $CH_4$ and $N_2O$ in air extracted by sublimation from Antarctica ice cores: confirmation of the data obtained using other extraction techniques, J. Geophys. Res., 103, 15971–15978, 1998.

Ikeda, T., Fukazawa, H., Mae, S., Pépin, L., Duval, P., Champagnon, B., Lipenkov, V. Y., and Hondoh, T.: Extreme fractionation of gases caused by formation of clathrate hydrates in Vostok Antarctic ice, Geophys. Res. Lett., 26, 91–94, 1999.

Indermühle, A., Stocker, T. F., Fischer, H., Smith, H. J., Joos, F., Wahlen, M., Deck, B., Mastroianni, D., Tschumi, J., Blunier, T., Meyer, R., and Stauffer, B.: Holocene carbon-cycle dynamics based on $CO_2$ trapped in ice at Taylor Dome, Antarctica, Nature, 398, 121–126, 1999.

Johnsen, S., Dahl-Jensen, D., Dansgaard, W., and Gundestrup, N.: Greenland palaeotemperatures derived from GRIP bore hole temperature and ice core isotope profiles, Tellus B, 47, 624–629, 1995.

Kawamura, K., Nakazawa, T., Aoki, S., Sugawara, S., Fujii, Y., and Watanabe, O.: Atmospheric $CO_2$ variations over the last three glacial–interglacial climatic cycles deduced from the Dome Fuji deep ice core, Antarctica using a wet extraction technique, Tellus B, 55, 126–137, 2003.

Köhler, P., Fischer, H., Schmitt, J., and Munhoven, G.: On the application and interpretation of Keeling plots in paleo climate research – deciphering $\delta^{13}C$ of atmospheric $CO_2$ measured in ice cores, Biogeosciences, 3, 539-556, doi:10.5194/bg-3-539-2006, 2006.

Leuenberger, D.: Highly resolved measurements of $\delta^{13}C$ on $CO_2$ extracted from an EPICA Dome C ice core, Master Thesis, Division for Climate and Environmental Physics, Physics Institute and Oeschger Centre for Climate Change Research, University of Bern, 2009.

Lourantou, A.: Constraints on the carbon dioxide deglacial rise based on its stable carbon isotopic ratio, Ph.D. thesis, doi: Univ. Joseph Fourier, Grenoble, France, 2009. Univ. Joseph Fourier, Grenoble, France, Univ. Joseph Fourier, Grenoble, France, 2009.

Lourantou, A., Chappellaz, J., Barnola, J. M., Masson-Delmotte, V., and Raynaud, D.: Changes in atmospheric $CO_2$ and its carbon isotopic ratio during the penultimate deglaciation, Quaternary Sci. Rev., 29, 1983–1992, doi:10.1016/j.quascirev.2010.05.002, 2010a.

Lourantou, A., Lavric, J. V., Kohler, P., Barnola, J. M., Paillard, D., Michel, E., Raynaud, D., and Chappellaz, J.: Constraint of the $CO_2$ rise by new atmospheric carbon isotopic measurements during the last deglaciation, Global Biogeochem. Cy., 24, Gb2015, doi:10.1029/2009gb003545, 2010b.

Lüthi, D., Le Floch, M., Bereiter, B., Blunier, T., Barnola, J.-M., Siegenthaler, U., Raynaud, D., Jouzel, J., Fischer, H., and Kawamura, K.: High-resolution carbon dioxide concentration record 650,000–800,000 years before present, Nature, 453, 379–382, 2008.

Lüthi, D.: $CO_2$ Konzentrationsmessungen an antarktischen Eisohrkernen: Natürliche Variabilität der letzten 800'000 Jahre und deren Zuverlässigkeit in Anbetracht von Prozessen im Eis, Dissertation, Physikalisches Institut, Abteilung Klima- und Umweltphysik, University of Bern, 160 pp., 2009.

MacFarling Meure, C., Etheridge, D., Trudinger, C., Steele, P., Langenfelds, R., van Ommen, T., Smith, A., and Elkins, J.: Law Dome $CO_2$, $CH_4$ and $N_2O$ ice core records extended to 2000 years BP, Geophys. Res. Lett., 33, L14810, doi:10.1029/2006GL026152, 2006.

Meijer, H. A. J.: The isotopic composition of the Groningen GS-19 and GS-20 pure $CO_2$ standards, in Reference and intercomparison materials for stable isotopes of lightelements, IAEA-TECDOC-825, 81–83, International Atomic Energy Agency, Vienna, 1995.

Neftel, A., Oeschger, H., Schwander, J., Stauffer, B., and Zumbrunn, R.: Ice core sample measurements give atmospheric $CO_2$ content during the past 40,000 yr, Nature, 295, 220–223, 1982.

Pearman, G. I., Etheridge, D., de Silva, F., and Fraser, P. J.: Evidence of changing concentrations of atmospheric $CO_2$, $N_2O$ and $CH_4$ from air bubbles in Antarctic ice, Nature, 320, 248–250, 1986.

Rubino, M., Etheridge, D. M., Trudinger, C. M., Allison, C. E., Battle, M. O., Langenfelds, R. L., Steele, L. P., Curran, M., Bender, M., White, J. W. C., Jenk, T. M., Blunier, T., and Francey, R. J.: A revised 1000-year atmospheric $\delta^{13}C$-$CO_2$ record from Law Dome and South Pole, Antarctica, J. Geophys. Res.-Atmos., 118, 8482–8499, doi:10.1002/jgrd.50668, 2013.

Schaefer, H., Lourantou, A., Chappellaz, J., Lüthi, D., Bereiter, B., and Barnola, J.-M.: On the suitability of partially clathrated ice for analysis of concentration and $\delta^{13}C$ of palaeo-atmospheric $CO_2$, Earth Planet. Sc. Lett., 307, 334–340, doi:10.1016/j.epsl.2011.05.007, 2011.

Schmitt, J.: A sublimation technique for high-precision $\delta^{13}C$ on $CO_2$ and $CO_2$ mixing ratio from air trapped in deep ice cores, Dissertation, University of Bremen, 2006.

Schmitt, J., Schneider, R., and Fischer, H.: A sublimation technique for high-precision measurements of $\delta^{13}CO_2$ and mixing ratios of $CO_2$ and $N_2O$ from air trapped in ice cores, Atmos. Meas. Tech., 4, 1445–1461, doi:10.5194/amt-4-1445-2011, 2011.

Schmitt, J., Schneider, R., Elsig, J., Leuenberger, D., Lourantou, A., Chappellaz, J., Köhler, P., Joos, F., Stocker, T. F., Leuenberger, M., and Fischer, H.: Carbon isotope constraints on the deglacial

$CO_2$ rise from ice cores, Science, 336, 711–714, 10.1126/science.1217161, 2012.

Schneider, R., Schmitt, J., Köhler, P., Joos, F., and Fischer, H.: A reconstruction of atmospheric carbon dioxide and its stable carbon isotopic composition from the penultimate glacial maximum to the last glacial inception, Clim. Past, 9, 2507–2523, doi:10.5194/cp-9-2507-2013, 2013.

Siegenthaler, U., Friedli, H., Loetscher, H., Moor, E., Neftel, A., Oeschger, H., and Stauffer, B.: Stable-isotope ratios and concentration of $CO_2$ in air from polar ice cores, Ann. Glaciol., 10, 151–156, 1988.

Smith, H. J., Fischer, H., Wahlen, M., Mastroianni, D., and Deck, B.: Dual modes of the carbon cycle since the Last Glacial Maximum, Nature, 400, 248–250, doi:10.1038/22291, 1999.

Sowers, T. and Jubenville, J.: A modified extraction technique for liberating occluded gases from ice cores, J. Geophys. Res.-Atmos., 105, 29155–29164, 2000.

Sperlich, P., Buizert, C., Jenk, T. M., Sapart, C. J., Prokopiou, M., Röckmann, T., and Blunier, T.: An automated GC-C-GC-IRMS setup to measure palaeoatmospheric $\delta^{13}$C-$CH_4$, $\delta^{15}$N-$N_2O$ and $\delta^{18}$O-$N_2O$ in one ice core sample, Atmos. Meas. Tech., 6, 2027–2041, doi:10.5194/amt-6-2027-2013, 2013.

Stauffer, B., Fischer, G., Neftel, A., and Oeschger, H.: Increase of Atmospheric Methane Recorded in Antarctic Ice Core, Science, 229, 1386–1388, 1985.

Stowasser, C., Buizert, C., Gkinis, V., Chappellaz, J., Schüpbach, S., Bigler, M., Faïn, X., Sperlich, P., Baumgartner, M., Schilt, A., and Blunier, T.: Continuous measurements of methane mixing ratios from ice cores, Atmos. Meas. Tech., 5, 999–1013, doi:10.5194/amt-5-999-2012, 2012.

Sturm, P., Leuenberger, M., Sirignano, C., Neubert, R., Meijer, H., Langenfelds, R., Brand, W., and Tohjima, Y.: Permeation of atmospheric gases through polymer O-rings used in flasks for air sampling, J. Geophys. Res.-Atmos., 109, D04309, doi:10.1029/2003/JD004073, 2004.

Tans, P. P. and Zhao, C. L.: Maintenance and propagation of the WMO mole fraction scale for carbon dioxide in air, 12th WMO/IAEA Meeting of Experts on Carbon Dioxide Concentration and Related Tracer Measurements Techniques, World Meteorological Organisation, Toronto, Ontario, Canada, 2003.

Uchida, T., Hondoh, T., Mae, S., Shoji, H., and Azuma, N.: Optimized storage condition of deep ice core samples from the viewpoint of air-hydrate analysis, Mem. Natl Inst. Polar Res., Spec. Issue 49, 306–313, 1994.

Werner, R. A. and Brand, W. A.: Referencing strategies and techniques in stable isotope ratio analysis, Rapid Commun. Mass Sp., 15, 501–519, 2001.

Zhang, J., Quay, P. D., and Wilbur, D. O.: Carbon isotope fractionation during gas-water exchange and dissolution of $CO_2$, Geochim. Cosmochim. Acta, 59, 107–114, 1995.

Zhao, C. L. and Tans, P. P.: Estimating uncertainty of the WMO mole fraction scale for carbon dioxide in air, J. Geophys. Res.-Atmos., 111, D08S09, doi:10.1029/2005JD006003, 2006.

Zumbrunn, R., Neftel, A., and Oeschger, H.: $CO_2$ measurements on 1-$cm^3$ ice samples with an IR laserspectrometer (IRLS) combined with a new dry extraction device, Earth Planet. Sc. Lett., 60, 318–324, 1982.